Mathematical Biosciences 387 (2025) 109499

Contents lists available at ScienceDirect

Mathematical Biosciences

journal homepage: www.elsevier.com/locate/mbs

Original Research Article

Assessing the influence of HIV on the spread of Mpox disease

Arsène Jaurès Ouemba Tassé [a,b,*], Yibetal Terefe [c], Jean Lubuma [a]

[a] School of Computer Science and Applied Mathematics, University of the Witwatersrand, Johannesburg, South Africa
[b] Mathematics and Applications Research Unit, University of Dschang, Dschang, Cameroon
[c] Department of Mathematics and Applied Mathematics, University of the Free State, Bloemfontein, South Africa

ARTICLE INFO

MSC:
34C60
37N25
37N30
65L12

Keywords:
Mpox
People infected with HIV
Stability of Equilibria
Target reproduction number
Model calibration
Nonstandard finite difference scheme

ABSTRACT

Mpox, originating primarily in African rodents, has led to human outbreaks over recent years. This study presents a mathematical model for Mpox, distinguishing between individuals with and without HIV who are susceptible. We explore scenarios involving both rodent-to-human transmission and those without it. In the absence of this transmission route, the model undergoes a backward bifurcation, suggesting that reducing the basic reproduction number below one would not eliminate the disease unless further control strategies are used. With the account of rodent-to-human transmission, if Mpox is endemic in the rodent population, a unique interior equilibrium, globally asymptotically stable, exists, requiring targeted interventions like quarantine or vaccination for people with HIV (PWH) for disease control. Model validation using USA case data (May 2022–July 2024) shows that both human-to-human and rodent-to-human transmissions prevail in the population, but the disease is not endemic. Projections indicate that the outbreak will be overcome by May 2027, with a total of 35,811 cases. We design a nonstandard finite difference (NSFD) scheme which is dynamically consistent with respect to the qualitative properties of the continuous model. Numerical simulations demonstrate that reducing the recruitment rate of PWH is essential, and rodent-to-human transmission is identified as highly influential in increasing the number of Mpox cases.

1. Introduction

Mpox is a viral disease caused by the Mpox virus, a species of the genus Orthopoxvirus [1]. Initially present in animals, particularly African rodents, the virus has now spread to humans. The disease has an incubation period of 1–21 days, during which individuals do not transmit the infection. Mpox resembles a milder form of smallpox, with less severe symptoms and lower lethality [2].

Common symptoms include rash, fever, sore throat, headache, muscle aches, back pain, low energy, and swollen lymph nodes. The severity of the rash can vary, with some individuals having only a few lesions, while others may develop hundreds. Transmission occurs through direct contact with infected animals (such as rodents, prairie dogs, and mice [3,4]), through contact with skin lesions or bodily fluids, or indirectly via contaminated materials like bedding or surfaces [5].

During the 2022 outbreak, some researchers identified sexual activity and direct contact with saliva or seminal fluid as primary transmission routes [6]. Treatment focuses on managing symptoms such as rash and pain, as well as preventing complications. Antivirals such as tecovirimat, originally developed for smallpox, have shown partial effectiveness against Mpox, although further studies are ongoing [1].

The JYNNEOS vaccine, produced by Bavarian Nordic, was the only vaccine used in the USA during the 2022 Mpox outbreak [6]. However, mass vaccination was not recommended [7].

On July 23, 2022, the World Health Organization (WHO) declared Mpox a Public Health Emergency of International Concern (PHEIC) for the first time [8]. Two years later, on August 13 and 14, 2024, both the Centers for Disease Control and Prevention (CDC) and the WHO once again declared Mpox a PHEIC due to its rapid global spread in countries where the virus had not previously been detected [9]. These declarations marked the highest alarm levels issued by the WHO within two years, and the disease continues to spread. From January to August 2024, more than 15,600 cases were reported in the Democratic Republic of Congo (DRC), resulting in 537 deaths. This underscores the urgent need to understand the dynamics of Mpox transmission to develop effective control measures.

Researchers worldwide have established a significant correlation between HIV and Mpox [6,10,11]. In the USA and Europe, it has been shown that between 40% and 90% of Mpox cases occurred in people with HIV (PWH) [6]. These individuals have higher hospitalization rates compared to those without HIV, due to their weakened immune

* Corresponding author at: School of Computer Science and Applied Mathematics, University of the Witwatersrand, Johannesburg, South Africa.
E-mail address: arsene.ouembatasse@wits.ac.za (A.J. Ouemba Tassé).

https://doi.org/10.1016/j.mbs.2025.109499
Received 28 December 2024; Received in revised form 6 June 2025; Accepted 16 June 2025
Available online 29 June 2025

systems. Notably, a necrotizing form of Mpox with a high fatality rate has been observed in individuals with advanced HIV [11]. The review [10] highlights that HIV-Mpox co-infection is particularly dangerous because it exacerbates symptoms of both diseases, complicating treatment. Given that PWH are disproportionately affected in current Mpox cases and deaths [12], it is crucial to incorporate HIV-infected individuals into Mpox models to better understand disease dynamics and evaluate the effectiveness of control strategies.

To date, some studies have addressed the dynamics of Mpox through mathematical modeling, incorporating the spillover event from rodents to humans [13–19] and some research papers dealt with HIV co-infection with other diseases [18,20–23], including Mpox. In particular, the work in [18,22] addressed HIV-Mpox co-infection models within the male homosexual population. The findings in these studies suggest that Mpox infection confers HIV-cross-immunity i.e., individuals who contracted Mpox cannot be infected by HIV during their whole life, meaning that Mpox infection serves as a preventive measure against HIV transmission, which is questionable. The purpose of this work is to fill this gap. More precisely, we target PWH, disproportionately infected by Mpox, due to their weakened immune systems.

Specifically, we propose a two-group model: one group represents individuals without HIV, and the other group represents individuals with HIV. Unlike the first group, which may present a moderate form of the disease, the second group exhibits only a severe form of Mpox that needs intervention. The model incorporates human-to-human, rodent-to-human, and rodent-to-rodent transmission. Moreover, it is quantitatively and qualitatively analyzed, and is calibrated using real data from the USA between May 10, 2022, and July 09, 2024.

Given the rich and the complex dynamics of the problem at hand, we have opted to use the nonstandard finite difference (NSFD) scheme, which has shown great potential in preserving the qualitative properties of the involved continuous model irrespective of the value of the step size [24,25]. We therefore construct a NSFD scheme that is dynamically consistent. Numerical simulations, supporting the theoretical findings such as the stability of the model equilibria and the sensitivity of its parameters, are conducted using this scheme.

The rest of the paper is structured as follows: In Section 2, details of the model formulation are given. Section 3 presents the quantitative and qualitative analysis of the model, including the calculation of the target reproduction number when only susceptible individuals with HIV are targeted. A special case of the full model is discussed in Section 4. Section 5 addresses model calibration and outbreak forecasting. The NSFD scheme and numerical simulations are presented in Section 6. Section 7 provides concluding remarks on how our findings fit into the literature and perspectives for future work.

2. Model formulation

Studying the dynamics of Mpox, particularly among PWH, is essential for understanding and predicting the disease's progression, as infections predominantly occur within this group. While a co-infection model incorporating both HIV and Mpox could address this issue, we adopt a two-group approach for clarity. We make the following assumptions:

- A.1 People living with HIV are assumed to develop only the critical form of the disease [26]. Additionally, infected people of this category are assumed to receive medical assistance to recover. This assumption is based on the compromised immune systems of many individuals in this group (about 91% of Mpox-infected PWH have a CD4 cell count of less than 350 cells per mm^3 [6]).
- A.2 Individuals without HIV can contract either a moderate or a severe form of the disease. The "moderate form" refers to the form that goes away by its own or within a few weeks after supportive care, such as painkiller or fever medication [27,28]. We assume that infected individuals with moderate Mpox form do not die from the disease.
- A.3 There is no vertical transmission of Mpox.
- A.4 The recovered Mpox cases are permanently immune [17,19].
- A.5 Human-to-rodent transmission will be neglected [13].
- A.6 Rodents act as the reservoir for the Mpox virus, meaning they carry and transmit the virus without recovering or dying from it. This assumption is consistent with the findings in [13].
- A.7 The Mpox latent period is neglected in both human and rodent populations.
- A.8 We gather all Mpox recovered individuals in the same compartment.
- A.9 While infected with Mpox, individuals do not contract HIV. This assumption is motivated by the fact that the Mpox infectious period lasts less than a month, which is quite short to contract HIV infection [18,22].
- A.10 Moderate Mpox cases do not evolve to a severe form of the disease. This assumption is consistent with the definition of moderate cases used in this work.
- A.11 We consider a linear transition from the HIV-uninfected susceptible compartment to the HIV-susceptible compartment. This assumption is made to forecast the current spread of Mpox in the USA.

2.1. Model variables and equation derivation

The human population is subdivided into the following compartments:

- $S_1 := S_1(t)$: HIV uninfected individuals susceptible to Mpox infection.
- $S_2 := S_2(t)$: HIV infected individuals susceptible to Mpox infection.
- $I_m := I_m(t)$: Asymptomatic and mild Mpox infected individuals. The incorporation of this compartment is in line with several studies that highlight that many Mpox-infected individuals are asymptomatic and several infected only have a moderate form of the disease [1,4,6].
- $I_s := I_s(t)$: Severe Mpox cases. Unlike the individuals in I_m, the infected individuals in I_s can succumb to the disease at a constant rate τ.
- $R := R(t)$: Mpox recovered individuals. Since we focus on the dynamics of Mpox and not that of HIV, it is relevant to assume that the R compartment encompasses both those infected with and without HIV who recovered from Mpox.

Likewise, the rodent population is divided into disjoint compartments:

- $S_r := S_r(t)$: Mpox susceptible rodents.
- $I_r := I_r(t)$: Mpox infected rodents.

We set

$$N_h := N_h(t) = S_1 + S_2 + I_m + I_s + R, \quad \text{and} \quad N_r := N_r(t) = S_r + I_r,$$

the total populations of humans and rodents, respectively.

Infection is modeled by standard incidence. The force of infection in the human population is defined as

$$\lambda = \frac{\beta_h(I_m + \nu_s I_s)}{N_h} + \frac{\omega I_r}{N_r},$$

where β and ω are the effective transmission rates from I_m and I_r to the susceptible in S_1, respectively, and ν_s is the modification parameter for the infectiousness of individuals in I_s compared to those in I_m.

We define the force of infection in the rodent population as

$$\lambda_r = \frac{\beta_r I_r}{N_r},$$

with β_r the rodent-to-rodent transmission rate.

Table 1
Variables and parameters description.

Variable	Description
S_1	Mpox susceptible individuals without HIV.
S_2	Mpox susceptible individuals with HIV.
I_m	Moderate Mpox cases.
I_s	Severe Mpox infected cases.
R	Mpox recovered individuals
S_r	Mpox susceptible rodents.
I_r	Mpox infected rodents.
Parameter	**Description**
Λ	Recruitment constant rate of the human population .
Λ_r	Recruitment constant rate of the rodent population.
p	Proportion of susceptible individuals recruited in the compartment S_1.
θ	Exit rate from the compartment S_1 to the compartment S_2.
$\beta_h(\omega)$	Effective transmission rate of Mpox in the human population due to individuals in the compartment $I_m(I_r)$.
ν_s	Modification parameter for the infectiousness of individuals in I_s.
β_r	Effective transmission rate of Mpox in the rodent population.
q	Proportion of individuals in S_1 who develop a mild form of Mpox when they are infected.
σ	Modification parameter that accounts for the increased susceptibility of the individuals in S_2 as compared to those in S_1.
$\gamma_m(\gamma_s)$	Recovery rate in the compartment $I_m(I_s)$.
δ	Additional death rate in the S_2 compartment due to HIV's infection.
τ	Average additional death rate in I_s due to the severity of Mpox and eventually the co-morbidity of some of these individuals.
μ	Natural mortality rate of humans.
η	Mortality rate in compartment R.
μ_r	Natural mortality rate of rodents.

2.2. Derivation of the transmission dynamics

The recruitment constant of susceptible humans through births and migrations is Λ. Among the recruited individuals, a proportion p is HIV-negative, and the remaining proportion is HIV-positive. Susceptible individuals can become infected at a rate determined by the force of infection λ. However, due to their weakened immune systems, individuals in group S_2, have an increased susceptibility by a factor of $1+\sigma$ compared to those in group S_1. Additionally, individuals in S_1 can acquire HIV at a rate θ, transitioning them to S_2. The natural death rate is denoted by μ, and individuals in S_2 experience an additional death rate δ due to HIV infection. The dynamics of S_1 and S_2 are described as follows:

$$\begin{cases} \dot{S}_1 = p\Lambda - \lambda S_1 - (\theta+\mu)S_1, \\ \dot{S}_2 = (1-p)\Lambda + \theta S_1 - \lambda(1+\sigma)S_2 - (\mu+\delta)S_2. \end{cases}$$

Upon infection, individuals move to I_m and I_s compartments, depending on whether they exhibit moderate or severe symptoms. In light of Assumption A.2, individuals in S_2 move directly to I_s upon infection. On the other hand, a proportion, q, of individuals in S_1 develops a benign form of the infection, while the remaining proportion develops a severe form. Those with moderate and severe infections can (i) recover at rates γ_m and γ_s, respectively, or (ii) die at rates μ and $\mu+\tau$, respectively. Here, τ represents the average additional death rate in I_s due to the severity of Mpox and the co-morbidities affecting some of these individuals. This results in the following dynamics for I_m and I_s.

$$\begin{cases} \dot{I}_m = q\lambda S_1 - (\gamma_m+\mu)I_m, \\ \dot{I}_s = (1-q)\lambda S_1 + \lambda(1+\sigma)S_2 - (\gamma_s+\mu+\tau)I_s. \end{cases}$$

The recovered individuals are gathered in compartment R. In this class, we denote the average mortality rate as η. It holds that

$$\eta \geq \mu \tag{1}$$

because R contains individuals who have recovered from Mpox, both with and without HIV. The dynamics of R is described by the following equation:

$$\dot{R} = \gamma_m I_m + \gamma_s I_s - \eta R.$$

The rodent population is replenished at a constant Λ_r through births. Rodents experience a natural mortality rate of μ_r. Additionally, susceptible rodents can become infected at the force of infection λ_r. Consequently, the dynamics of the rodent population are described by the following system of equations:

$$\begin{cases} \dot{S}_r = \Lambda_r - \lambda_r S_r - \mu_r S_r, \\ \dot{I}_r = \lambda_r S_r - \mu_r I_r. \end{cases}$$

We gather the definitions of model parameters in Table 1. The flow diagram of the model is illustrated in Fig. 1. Combining all the equations results in System (2):

$$\begin{cases} \dot{S}_1 = p\Lambda - \lambda S_1 - (\mu+\theta)S_1, \\ \dot{S}_2 = (1-p)\Lambda + \theta S_1 - \lambda(1+\sigma)S_2 - (\mu+\delta)S_2, \\ \dot{I}_m = q\lambda S_1 - (\mu+\gamma_m)I_m, \\ \dot{I}_s = (1-q)\lambda S_1 + \lambda(1+\sigma)S_2 - (\mu+\gamma_s+\tau)I_s, \\ \dot{R} = \gamma_m I_m + \gamma_s I_s - \eta R, \\ \dot{S}_r = \Lambda_r - \lambda_r S_r - \mu_r S_r, \\ \dot{I}_r = \lambda_r S_r - \mu_r I_r \end{cases} \tag{2}$$

System (2) is supplemented with the following non-negative initial conditions:

$$S_1(0) = S_1^0 \geq 0,\ S_2(0) = S_2^0 \geq 0,\ I_m(0) = I_m^0 \geq 0,\ I_s(0) = I_s^0 \geq 0,$$
$$R(0) = R^0 \geq 0,$$

$$S_r(0) = S_r^0 \geq 0 \text{ and } I_r(0) = I_r^0 \geq 0.$$

For mathematical convenience, we consider the definitions

$$\phi_1 = \mu+\theta, \quad \phi_2 = \mu+\delta, \ \phi_3 = \mu+\gamma_m, \quad \phi_4 = \mu+\gamma_s+\tau,$$
$$a_1 = p\Lambda, \quad a_2 = (1-p)\Lambda, \quad a_3 = 1+\sigma, \quad a_4 = 1-q.$$

The other parameters used in the manuscript will be defined upon their first appearance, and all of the parameters used are grouped in Appendix A.

3. Quantitative and qualitative analysis of the model

3.1. Well-posedness of the model

The following theorem shows that Model (2) is well-posed.

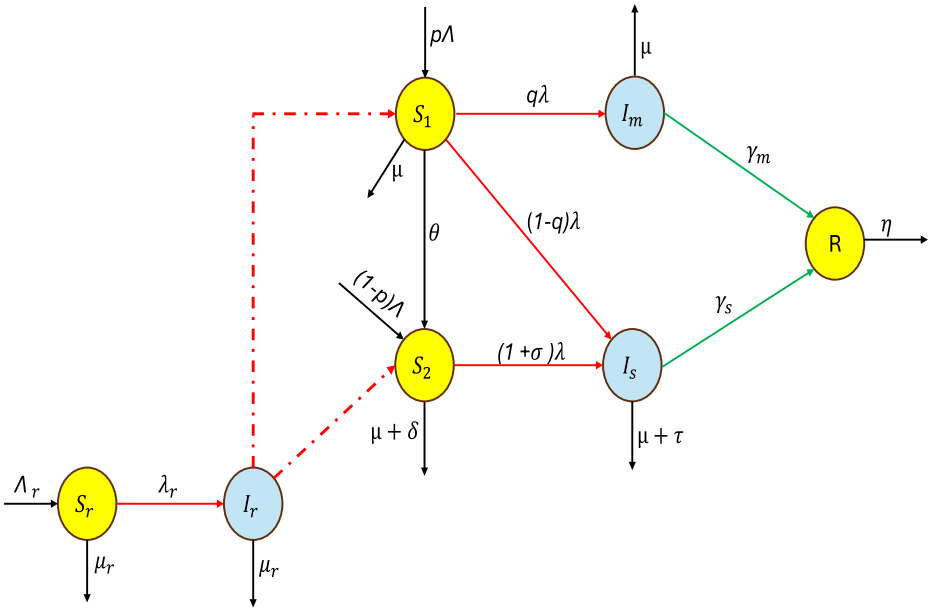

Fig. 1. Flow diagram of Model (2). Dashed lines represent interactions between susceptible humans and infected rodents. Solid lines depict movement between compartments: red arrows towards infected classes, green arrows towards recovery, and black arrows for recruitment, HIV infection, and death..

Theorem 3.1. *Model (2) is a dynamical system on the following biologically feasible region Ω which is attractive:*

$$\Omega = \Omega_h \times \Omega_r \subset \mathbb{R}^5_+ \times \mathbb{R}^2_+,$$

where

$$\Omega_h = \left\{ (S_1, S_2, I_m, I_s, R) \in \mathbb{R}^5_+ \,/\, N_h \leq \frac{\Lambda}{\mu} \right\},$$

$$\text{and} \quad \Omega_r = \left\{ (S_r, I_r) \in \mathbb{R}^2_+ \,/\, N_r \leq \frac{\Lambda_r}{\mu_r} \right\}.$$

Proof. Let

$$f := f(S_1, S_2, I_m, I_s, R, S_r, I_r) := (f_i)_{i=1,\ldots,7}$$

be the right-hand side of Model (2). Thanks to the Cauchy-Lipschitz theorem [29], System (2) admits a unique local solution.

Let $(S_1(t), S_2(t), I_m(t), I_s(t), R(t))$ be a solution of Model (2). Set

$$\psi_1(t) = \lambda(t) + \theta + \mu,\ \psi_r(t) = \lambda_r(t) + \mu_r, a(t) = \lambda(t)a_3 + \phi_2 \text{ and } b(t) = a_2 + \theta S_1(t).$$

By the integrating factor technique, it follows that

$$\begin{aligned}
S_1(t) &= S_1(0)\exp\left(\int_0^t -\psi_1(s)ds\right) + \exp\left(\int_0^t -\psi_1(s)ds\right) \\
&\quad \times \int_0^t \left(a_1 \exp\left(\int_0^u \psi_1(s)ds\right)\right) du \\
S_r(t) &= S_r(0)\exp\left(\int_0^t -\psi_r(s)ds\right) + \exp\left(\int_0^t -\psi_r(s)ds\right) \\
&\quad \times \int_0^t \left(\Lambda_r \exp\left(\int_0^u \psi_r(s)ds\right)\right) du \\
S_2(t) &= S_2(0)\exp\left(\int_0^t -a(s)ds\right) + \exp\left(\int_0^t -a(s)ds\right) \\
&\quad \times \int_0^t \left(b(s)\exp\left(\int_0^s a(u)du\right)\right) ds.
\end{aligned}$$

Thus, $S_1(t), S_2(t), S_r(t) \geq 0,\ \forall\, t > 0$ whenever $S_1(0), S_2(0), S_r(0) \geq 0$.

We use the barrier theorem for the variables I_m, I_s, R and I_r. The boundary of the positive cone $\mathbb{R}^4_+$ consists of the 4 hyperplanes $I_m = 0$, $I_s = 0$, $R = 0$, $I_r = 0$, each of which has u_l as the unit outer normal vector, $\{-u_l, l = 3, 4, 5, 7\}$ being the canonical basis of the space $\mathbb{R}^4$. For the hyperplane $I_m = 0$, we have

$$\langle u_3, f_3 \rangle = -q\lambda S_1 \leq 0.$$

Thus, according to the tangent condition, I_m remains non-negative when $I_m(0) \geq 0$. Similarly, it can be proved that the other variables of the model remain non-negative for non-negative initial conditions. Therefore, the set $\mathbb{R}^+_7$ is forward invariant with respect to Model (2).

Furthermore, assume

$$N_h(0) \leq \frac{\Lambda}{\mu} \text{ and } N_r(0) \leq \frac{\Lambda_r}{\mu_r}.$$

It is straightforward that

$$\dot{N}_h(t) \leq \Lambda - \mu N_h \text{ and } \dot{N}_r(t) = \Lambda_r - \mu_r N_r. \tag{3}$$

From Gronwall inequality, it follows that, for every $t \geq 0$,

$$N_h(t) \leq \frac{\Lambda}{\mu} + \left(N_h(0) - \frac{\Lambda}{\mu}\right) e^{-\mu t} \text{ and } N_r(t) = \frac{\Lambda_r}{\mu_r} + \left(N_r(0) - \frac{\Lambda_r}{\mu_r}\right) e^{-\mu_r t}.$$

Hence

$$\begin{aligned}
&N_h(t) \leq \frac{\Lambda}{\mu}, \forall\, t>0 \text{ and } \limsup_{t\longrightarrow+\infty} N_h(t) \leq \frac{\Lambda}{\mu}. \\
&N_r(t) \leq \frac{\Lambda_r}{\mu_r}, \forall\, t>0 \text{ and } \lim_{t\longrightarrow+\infty} N_r(t) = \frac{\Lambda_r}{\mu_r}.
\end{aligned}$$

This implies that Ω is positively invariant and attractive (see Theorem 2.1.5 in [30]). □

3.2. Basic reproduction number

Straightforward computations show that Model (2) has a disease-free equilibrium (DFE)

$$\mathcal{E}_0 := \left(\frac{a_1}{\phi_1}, \frac{a_5}{\phi_1\phi_2}, 0, 0, 0, \frac{\Lambda_r}{\mu_r}, 0\right) =: (S_{10}, S_{20}, 0, 0, 0, N_r^*, 0), \tag{4}$$

$$S_{10} = \frac{a_1}{\phi_1},\ \ S_{20} = \frac{a_5}{\phi_1\phi_2},\ \ N_r^* = \frac{\Lambda_r}{\mu_r},\ \ N_0 = S_{10} + S_{20};\ \text{and}\ a_5 = a_2\phi_1 + \theta a_1.$$

The basic reproduction number, $\mathcal{R}_0$, is defined as the number of secondary cases produced by one infected individual introduced in a completely susceptible population during its entire infectious period. Using the next generation method [31], we define by $\mathcal{F}$ and $\mathcal{V}$ the vectors of the new infections and the transition terms as:

$$\mathcal{F} = \begin{pmatrix} q\lambda S_1 \\ (1-q)\lambda S_1 + \lambda a_3 S_2 \\ \lambda_r S_r \end{pmatrix} \text{ and } \mathcal{V} = \begin{pmatrix} \phi_3 I_m \\ \phi_4 I_s \\ \mu_r I_r \end{pmatrix}, \text{ respectively.}$$

The Jacobian of these matrices at the DFE, denoted by F and V, given by

$$F = \begin{pmatrix} \frac{q\beta_h S_{10}}{N_0} & \frac{q\nu_s\beta_h S_{10}}{N_0} & \frac{q\omega S_{10}}{N_r^*} \\ \frac{\beta_h((1-q)S_{10}+a_3S_{20})}{N_0} & \frac{\beta_h\nu_s((1-q)S_{10}+a_3S_{20})}{N_0} & \frac{\omega((1-q)S_{10}+a_3S_{20})}{N_r^*} \\ 0 & 0 & \beta_r \end{pmatrix}$$

and

$$V = \begin{pmatrix} \phi_3 & 0 & 0 \\ 0 & \phi_4 & 0 \\ 0 & 0 & \mu_r \end{pmatrix},$$

respectively, are used to compute the basic reproduction number $\mathcal{R}_0 = \rho(K)$, where $K = FV^{-1}$, and $\rho(A)$ is defined as the spectral radius of a square matrix A.

Simple computations show that,

$$\begin{aligned} \mathcal{R}_0 &= \max\left\{ \frac{q\beta_h S_{10}}{\phi_3 N_0} + \frac{\beta_h\nu_s((1-q)S_{10}+a_3S_{20})}{\phi_4 N_0},\ \frac{\beta_r}{\mu_r} \right\} \\ &=: \max\{\mathcal{R}_0^H,\ \mathcal{R}_0^R\}, \end{aligned} \tag{5}$$

where

$$\mathcal{R}_0^H = \frac{q\beta_h S_{10}}{\phi_3 N_0} + \frac{\beta_h\nu_s((1-q)S_{10}+a_3S_{20})}{\phi_4 N_0} = \frac{a_{14}}{a_{12}} \quad \text{and} \quad \mathcal{R}_0^R = \frac{\beta_r}{\mu_r},$$

with a_{12} and a_{14} defined in Eq. (6).

$\mathcal{R}_0^R$ is the basic reproduction number for the rodents-only Mpox model defined in Eq. , and $\mathcal{R}_0^H$ is the basic reproduction number for the humans-only Mpox model defined in Eq. (14). The first term of $\mathcal{R}_0^H$ is the contribution of moderate cases to the transmission of Mpox, while the second term is the contribution of severe cases.

The result below comes from [31].

Theorem 3.2. *The DFE is locally asymptotically stable if $\mathcal{R}_0 < 1$ and unstable when $\mathcal{R}_0 > 1$.*

In light of the expression of $\mathcal{R}_0$, an epidemic can occur if either $\mathcal{R}_0^H > 1$ or $\mathcal{R}_0^R > 1$. Nevertheless, it is worth noting that the disease can disappear in the rodent population while persisting in the human population. However, the inverse is impossible due to spillover events from rodents to humans. Further explanation will be provided in numerical simulations (see Fig. 7 and related comments).

3.3. Positive equilibria of model (2)

Let $(S_1^*, S_2^*, I_m^*, I_s^*, R^*, S_r^*, I_r^*)$ be any equilibrium of Model (2), i.e, a root of the right-hand side of the model. Set

$$\begin{aligned} &a_6 = a_1a_4a_3 + a_2a_3, \quad a_7 = a_1a_4\phi_2 + a_3a_5, \quad a_8 = \gamma_m q a_1 a_3\phi_4 + \phi_3\gamma_s a_6, \\ &a_9 = \gamma_m q a_1\phi_2\phi_4 + \phi_3\gamma_s a_7, \quad a_{10} = a_8 + a_6\eta\phi_3 + q a_1\eta\phi_4 a_3, \\ &a_{11} = a_7\eta\phi_3 + a_9 + q a_1\eta\phi_2\phi_4 + a_2\eta\phi_3\phi_4 + a_1\eta a_3\phi_3\phi_4, \\ &a_{12} = a_1\eta\phi_2\phi_3\phi_4 + a_5\eta\phi_3\phi_4, \\ &a_{13} = \beta_h q a_1\eta\phi_4 a_3 + a_6\eta\phi_3\beta_h\nu_s, \quad a_{14} = \beta_h q a_1\eta\phi_4\phi_2 + a_7\eta\phi_3\beta_h\nu_s. \end{aligned} \tag{6}$$

Let us denote by λ^* and λ_r^* the forces of infection λ and λ_r at the equilibrium point. Setting the right-hand side of Model (2) equals to zero, we get after some algebra

$$\begin{aligned} &S_1^* = \frac{a_1}{\lambda^*+\phi_1},\ S_2^* = \frac{a_2\lambda^*+a_5}{(\lambda^*+\phi_1)(a_3\lambda^*+\phi_2)},\ I_m^* = \frac{q a_1\lambda^*}{(\lambda^*+\phi_1)\phi_3}, \\ &I_s^* = \frac{a_6\lambda^{*2}+a_7\lambda^*}{\phi_4(\lambda^*+\phi_1)(a_3\lambda^*+\phi_2)}, \qquad R^* = \frac{a_8\lambda^{*2}+a_9\lambda^*}{\eta\phi_3\phi_4(\lambda^*+\phi_1)(a_3\lambda^*+\phi_2)}, \\ &S_r^* = \frac{\Lambda_r}{\mu_r+\lambda_r^*},\ I_r = \frac{\Lambda_r\lambda_r^*}{\mu_r(\mu_r+\lambda_r^*)}, \qquad N_h^* = \frac{a_{10}\lambda^{*2}+a_{11}\lambda^*+a_{12}}{\eta\phi_3\phi_4(\lambda^*+\phi_1)(a_3\lambda^*+\phi_2)}. \end{aligned} \tag{7}$$

3.3.1. Positive frontier equilibria

An equilibrium is said frontier if at least one of its components is zero. A non-frontier equilibrium is called an interior or an endemic equilibrium.

Assume $I_r^* = 0$. Then, λ^* becomes

$$\lambda^* = \frac{(\lambda^*)^2 a_{13} + \lambda^* a_{14}}{a_{10}(\lambda^*)^2 + a_{11}\lambda^* + a_{12}}. \tag{8}$$

Thus, from (8), we infer $\lambda^* = 0$ or λ^* is solution to the equation

$$a_{10}(\lambda^*)^2 + (a_{11} - a_{13})\lambda^* + a_{12}\left(1 - \mathcal{R}_0^H\right) = 0. \tag{9}$$

$\lambda^* = 0$ refers to the DFE $\mathcal{E}_0$ at (4).

Based on Descartes's rule of signs, one has the following result regarding the existence of positive frontier equilibria for Model (2).

Theorem 3.3. *Model (2) has a unique frontier equilibrium, which is the human-only endemic equilibrium whenever $\mathcal{R}_0^H > 1$, while it has 0 or two positive frontier equilibria or human-only endemic equilibria when $\mathcal{R}_0^H < 1$.*

3.3.2. Interior equilibria

For an interior equilibrium for Model (2), we must have $I_r^* > 0$. In this case, some computations allow us to derive the relations

$$\lambda_r^* = \mu_r(\mathcal{R}_0^R - 1) \text{ and } I_r^* = \frac{\Lambda_r(\mathcal{R}_0^R - 1)}{\mu_r\mathcal{R}_0^R}. \tag{10}$$

Using Eq. (10), λ^* becomes

$$\lambda^* = \frac{(\lambda^*)^2 a_{13} + \lambda^* a_{14}}{a_{10}(\lambda^*)^2 + a_{11}\lambda^* + a_{12}} + \frac{\omega(\mathcal{R}_0^R - 1)}{\mathcal{R}_0^R}. \tag{11}$$

Further simplifications of (11) lead into

$$\mathcal{R}_0^R a_{10}(\lambda^*)^3 + (\lambda^*)^2 A_2 + \lambda^* A_1 - a_{12}\omega(\mathcal{R}_0^R - 1) = 0, \tag{12}$$

where

$$A_1 = \mathcal{R}_0^R a_{12}\left(1 - \mathcal{R}_0^H\right) - \omega a_{11}(\mathcal{R}_0^R - 1) \text{ and } A_2 = \mathcal{R}_0^R(a_{11} - a_{13}) - \omega a_{10}(\mathcal{R}_0^R - 1).$$

Thus, by Descartes's rule of signs, Model (2) admits at least one positive equilibrium when $\mathcal{R}_0^R > 1$, while it might have 0 endemic equilibrium if $\mathcal{R}_0^R < 1$. Using the third-degree polynomial (12) in λ^* and Descartes's rule of signs, we infer the following theorem about the existence of endemic equilibria.

Theorem 3.4. *Model (2) has at least one interior equilibrium when $\mathcal{R}_0^R > 1$. More precisely,*

1. *When $A_1.A_2 > 0$ or $A_1 < 0, A_2 > 0$, Model (2) has a unique interior equilibrium.*
2. *When $A_1 > 0, A_2 < 0$, Model (2) has one or three interior equilibria.*

Remark 3.5. It is difficult to determine theoretically the exact number of solutions of Eq. (12) when $\mathcal{R}_0^R > 1$, but numerically, for different sets of parameter values, we conjecture that Eq. (12) has a unique positive solution. A particular case is illustrated in Fig. 2, which plots only the positive solutions for Eq. (12) when $\mathcal{R}_0^R > 1$.

Moreover, one can easily see that the DFE $\mathcal{E}_0^r = (N_r^*, 0)$ of the rodent-only model is globally asymptotically stable (GAS) when $\mathcal{R}_0^R \le 1$ and it is unstable when $\mathcal{R}_0^R > 1$. In the latter case, the model admits a unique endemic equilibrium $\mathcal{E}_r^* = (S_r^*, I_r^*)$, with I_r^* given in Eq. 2 and $S_r^* = N_r^* - I_r^*$. Furthermore, $\mathcal{E}_r^*$ is GAS when $\mathcal{R}_0^R > 1$. The formal proof of this result is similar to the one provided in [32] for the Ebola disease.

3.4. Global stability of the DFE

The epidemiological implication of Theorem 3.2 is that Mpox can be eliminated in the human and rodent population when $\mathcal{R}_0 < 1$, provided

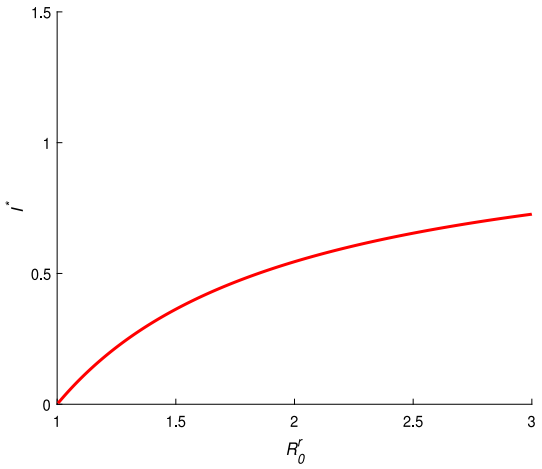

Fig. 2. Positive solutions for Eq. (12) when $\mathcal{R}_0^R > 1$: This figure is plotted with $\mu = 100.01; \theta = 0.02; \delta = 0.003; \gamma_m = 1000.03; \gamma_s = 10.0090; \tau = 22.01; p = 0.00008; \Lambda = 0.010; \sigma = 0.003; q = 0.4; \eta = 0.0003; \beta_h = 0.03; \nu_s = 0.02; \beta_r = 0.03; \omega = 1.09$.

that the initial conditions of Model (2) are in the basin of attraction of the DFE. For an effective control of the disease, we need to prove the global asymptotic stability of the DFE on Ω. To obtain this result, we introduce another threshold

$$\mathcal{N} = \max(\mathcal{N}_0, \mathcal{R}_0^R),$$

where

$$\mathcal{N}_0 = \mathcal{N}_1 + \mathcal{N}_2,\ \mathcal{N}_1 = \frac{(1-q)\beta_h\nu_s + a_3\beta_h\nu_s}{\phi_4},\ \mathcal{N}_2 = \frac{q\beta_h}{\phi_3(1-\mathcal{N}_1)}.$$

Theorem 3.6. *The DFE for Model (2) is globally asymptotically stable (GAS) provided that $\mathcal{N} < 1$.*

Proof. From the rodents conservation law in Eq. (3), we observe that N_r^* is GAS for the system $\dot{N}_r = \Lambda_r - \mu_r N_r$. Thus, to investigate the global asymptotic stability of $\mathcal{E}_0$, we can consider the asymptotically equivalent limiting system of System (2) where N_r is replaced by N_r^* [33,34].

Let us consider the candidate Lyapunov's function

$$L = I_m + c_1 I_s + c_2 I_r, \tag{13}$$

where c_1 and c_2 will be defined shortly. Some algebra show that, the derivative $\dot{L}$ of L along the trajectories of System (2) verifies

$$\begin{aligned}\dot{L} &\le q\beta_h(I_m + \nu_s I_s) + q\frac{\omega I_r S_{10}}{N_r^*} - \phi_3 I_m + c_1(1-q)\beta_h(I_m + \nu_s I_s) + c_1(1-q)\frac{\omega I_r S_{10}}{N_r^*}\\ &\quad + a_3 c_1\beta_h(I_m + \nu_s I_s) + a_3 c_1\frac{\omega I_r S_{20}}{N_r^*} - \phi_4 c_1 I_s + c_2\beta_r I_r - c_2\mu_r I_r\\ &\le I_m[q\beta_h - \phi_3 + c_1(1-q)\beta_h + a_3 c_1\beta_h] + I_s[q\beta_h\nu_s + c_1(1-q)\beta_h\nu_s + a_3 c_1\beta_h\nu_s\\ &\quad - \phi_4 c_1] + I_r\left[q\frac{\omega S_{10}}{N_r^*} + c_1(1-q)\frac{\omega S_{10}}{N_r^*} + a_3 c_1\frac{\omega S_{20}}{N_r^*} + c_2\beta_r - c_2\mu_r\right].\end{aligned}$$

We choose c_1 and c_2 such that

$$\begin{cases} q\beta_h\nu_s + c_1(1-q)\beta_h\nu_s + a_3 c_1\beta_h\nu_s - \phi_4 c_1 = 0\\ q\dfrac{\omega S_{10}}{N_r^*} + c_1(1-q)\dfrac{\omega S_{10}}{N_r^*} + a_3 c_1\dfrac{\omega S_{20}}{N_r^*} + c_2\beta_r - c_2\mu_r = 0.\end{cases}$$

Hence

$$c_1 = \frac{q\beta_s\nu_s}{\phi_4(1-\mathcal{N}_1)} \text{ and } c_2 = \frac{S_{10}(c_1\omega(1-q) + q\omega) + a_3 c_1\omega S_{20}}{\Lambda_r(1-\mathcal{R}_0^R)}.$$

This implies that

$$\dot{L} \le \phi_3 I_m(\mathcal{N}_2 - 1) \le \phi_3 I_m(\mathcal{N} - 1).$$

Thus, L is a strict Lyapunov function of Model (2) when $\mathcal{N} < 1$. Hence, the DFE is GAS by LaSalle's invariance principle [35]. □

Remark 3.7. Since $\mathcal{R}_0 \le \mathcal{N}$, Theorem 3.2 implies that achieving global control of Mpox requires more effort. Moreover, it is straightforward that when $\mathcal{R}_0^R < 1$, the disease will be eradicated in the rodent population. In this case, no interior equilibrium exists for Model (2). However, this does not guarantee disease elimination in the human population, as positive frontier equilibria may persist. Therefore, additional efforts are necessary to reduce $\mathcal{N}_0$ to a value less than one.

Mathematically, it is difficult to establish the stability of the endemic equilibrium. This important aspect will be addressed in some particular cases, while numerical simulations will be considered for the general case (see Section 6.2, Fig. 8).

3.5. Target reproduction number and control of the high-risk population group

The basic reproduction number, $\mathcal{R}_0$, provides an estimate of the severity of a disease and the effort required for its control. However, in multi-host or multi-group models, $\mathcal{R}_0$ becomes less relevant when control strategies, such as vector control or quarantine, are implemented at a particular host or group [36,37]. In such cases, the so-called target reproduction number is a more appropriate metric, as it quantifies the strength of control needed for a subset of hosts or groups.

Let $K = (k_{ij})_{1\le i,j\le n}$ be the next-generation matrix, with the usual understanding of its entries, namely k_{ij} represents the expected number of new cases that an infected individual of type j can caused among susceptible individuals of type i, in a fully susceptible population. Let $W = \{(i_1, j_1), \dots, (i_m, j_m)\}$ be the set of all targeted entries. Define the target matrix by

$$[K_w]_{ij} = \begin{cases} k_{ij}, & \text{if } (i,j) \in W,\\ 0, & \text{otherwise.}\end{cases}$$

The target reproduction number $\mathcal{T}$ is defined by [36,37]:

$$\mathcal{T} = \rho(K_w(I - K + K_w)^{-1}),\ \text{whenever } \mathcal{P} := \rho(K - K_w) < 1,$$

where I is the identity matrix.

When $\mathcal{T}$ is defined, it could serve as a relevant threshold for disease control. Furthermore, if K is irreducible, there exists a clear relationship between $\mathcal{T}$ and $\mathcal{R}_0$, as provided below in our specific Mpox model.

According to [10], Mpox occurs more frequently and is more virulent in PWH. Therefore, these individuals should be prioritized in the fight against the disease. This underscores the need to compute a relevant threshold for Mpox control when targeting only the susceptible individuals in the S_2 compartment (e.g., through measures aimed specifically at this group). Such targeted control strategies, referred to as S_2-control, may include quarantining susceptible individuals in S_2 [38] or vaccinating them with the JYNNEOS vaccine, which has been proven safe and effective for this population [39].

To implement the S_2-control, the target matrix K_w is defined as follows [40]:

$$K_w = \begin{pmatrix} 0 & 0 & 0\\ \dfrac{b_1\beta_h}{N_0} & \dfrac{b_2\nu_s\beta_h}{N_0} & \dfrac{b_3\omega}{\Lambda_r\mu_r^2}\\ 0 & 0 & 0\end{pmatrix},$$

where

$$b_1 = \frac{((1-q)S_{10} + a_3 S_{20})}{\phi_3},\ b_2 = \frac{((1-q)S_{10} + a_3 S_{20})}{\phi_4},\ \text{and}$$
$$b_3 = \frac{((1-q)S_{10} + a_3 S_{20})}{\mu_r}.$$

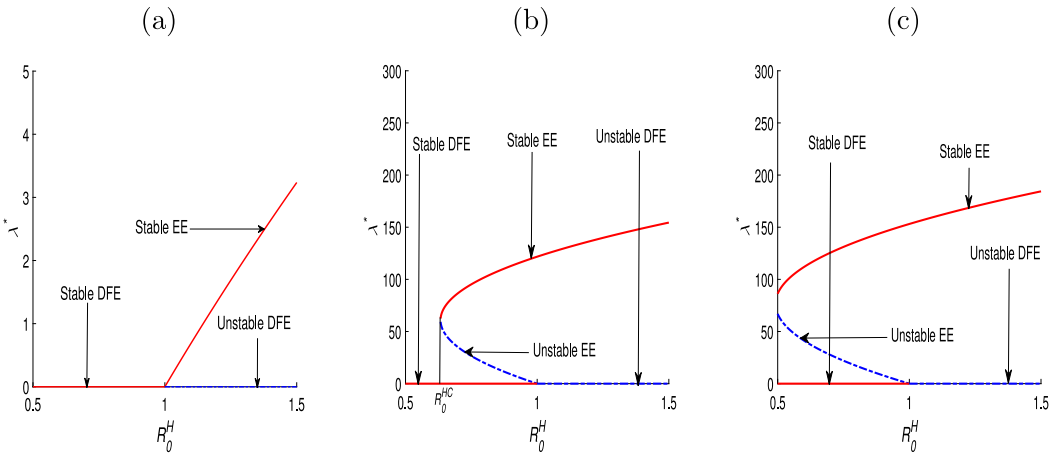

Fig. 3. Bifurcation diagrams for Model (14): (a) Left figure: forward bifurcation; (b) Middle figure: Backward bifurcation; (c) Right figure: Full backward bifurcation. Figure (a) is plotted with $\mu = 10.01; \theta = 0.000002; \delta = 0.03; \gamma_m = 0.00003; \gamma_s = 0.0090; \tau = 022.01; p = 0.02; \Lambda = 10; \sigma = 0.3; q = 0.4; \eta = 200.3; \beta_h = 1.3; \nu_s = 0.02$. Figure (b) is plotted with $\mu = 100.01; \theta = 0.002; \delta = 0.93; \gamma_m = 3.03; \gamma_s = 7.590; \tau = 6660.2201; p = 0.09; \Lambda = 10; \sigma = 0.3; q = 0.4; \eta = 0.3; \beta_h = 5000.03; \nu_s = 0.902$. Figure (c) is plotted with $\mu = 100.01; \theta = 0.002; \delta = 0.93; \gamma_s = 5.590$ (the other parameters are as in Figure (b)).

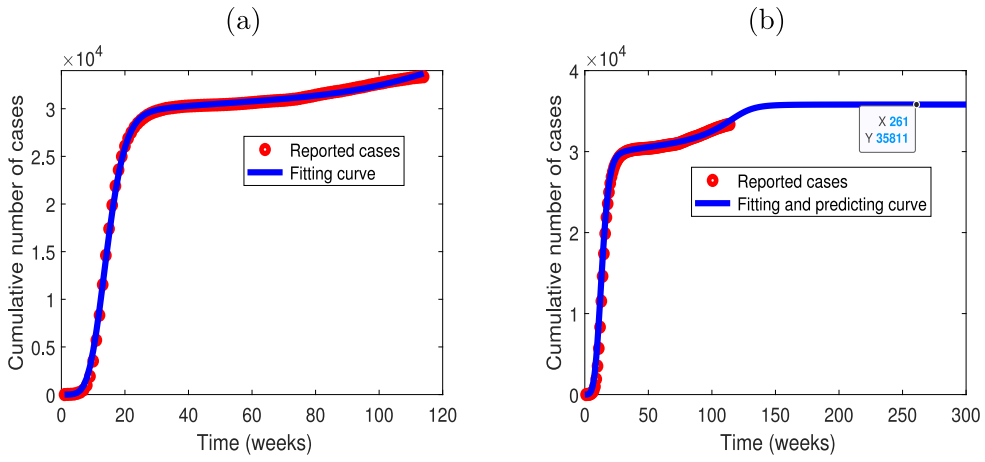

Fig. 4. Figure (a): Model calibration from the 10 May 2022 to 09 July 2024. Figure (b): Predicting curve up to 2028. The initial conditions are gathered in Table 2 and the parameter values are in Table 3.

Assume

$$\mathcal{P} := \rho(FV^{-1} - K_w) = \max\left(\frac{\beta_r}{\mu_r}, \frac{q\beta_h S_{10}}{\phi_3 N_0}\right) < 1.$$

Simple computations show that

$$\mathcal{T} = \rho(K_w(I - FV^{-1} + K_w)^{-1}) = \beta_h \nu_s \phi_3 b_2,$$

where I is the identity matrix.

This shows that $\mathcal{T}/\phi_3 = \beta_h \nu_s b_2$, i.e. $\mathcal{T}/\phi_3$ is the average number of effective contacts that could arise if a severe infected case is introduced into a completely susceptible population during he/she entire infectious period.

The announced relationships between the target/type reproduction number and the basic reproduction number read as follows [32,36,37]:

Theorem 3.8. *Assume $\mathcal{P} < 1$. Then one of the following statements holds.*

1. $1 < \mathcal{R}_0 < \mathcal{T}$, *or*
2. $\mathcal{T} = \mathcal{R}_0 = 1$, *or*
3. $\mathcal{T} < \mathcal{R}_0 < 1$.

Theorem 3.8 is due to the fact that the matrix FV^{-1} is irreducible [32,36,37]. This theorem points out that if $\mathcal{R}_0 > 1$ then $\mathcal{R}_0 < \mathcal{T}$, meaning that more effort is needed to control the disease through the S_2-control. In this case, the result below provides the minimum proportion of individuals in S_2 that should be controlled for eliminating the disease [36,37].

Proposition 3.9. *Assume $\mathcal{P} < 1$. If $\mathcal{T} > 1$, then Mpox can be overcome by targeting only the population in S_2. That is, the S_2-control is sufficient if a proportion $1 - \frac{1}{\mathcal{T}}$ of susceptible in S_2 is controlled.*

4. Model with only human-to-human transmission

Without the spillover event from rodents to humans, Model (2) becomes

$$\begin{cases} \dot{S}_1 = p\Lambda - \lambda S_1 - (\mu + \theta)S_1, \\ \dot{S}_2 = (1-p)\Lambda + \theta S_1 - \lambda(1+\sigma)S_2 - (\mu + \delta)S_2, \\ \dot{I}_m = q\lambda S_1 - (\mu + \gamma_m)I_m, \\ \dot{I}_s = (1-q)\lambda S_1 + \lambda(1+\sigma)S_2 - (\mu + \gamma_s + \tau)I_s, \\ \dot{R} = \gamma_m I_m + \gamma_s I_s - \eta R, \end{cases} \tag{14}$$

where

$$\lambda = \frac{\beta_h(I_m + \nu_s I_s)}{N_h}.$$

The existence of positive equilibria for Model (14) is a question of great interest, which we investigate based on the quadratic Eq. (9), rewritten for convenience in the form

$$A(\lambda^*)^2 + B\lambda^* + C\left(1 - \mathcal{R}_0^H\right) = 0. \tag{15}$$

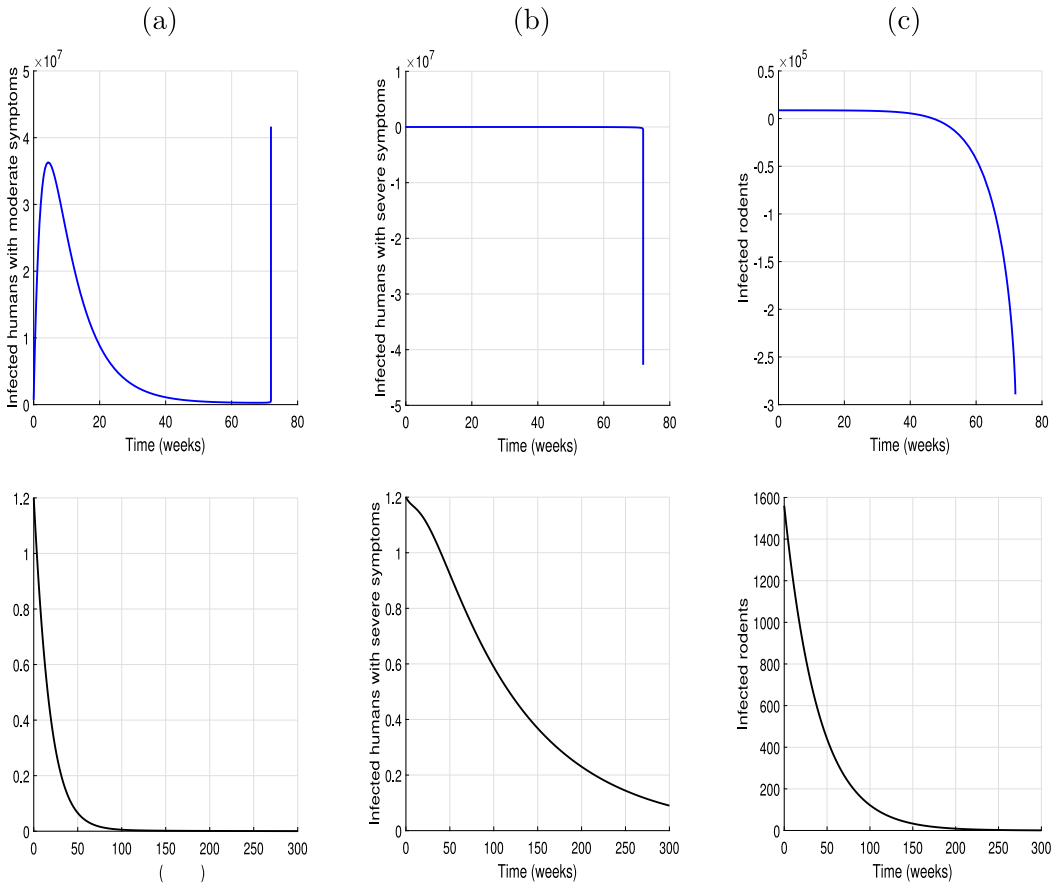

Fig. 5. Superiority of the NSFD scheme compared to ODE 45 with respect to the positivity of model variables. Top three figures: Solution curves for Model (2) using ODE 45. Bottom three figures: solution curves for Model (2) using the NSFD developed in System (20). This figure is plotted with $\beta_h = 0.23$ and $\omega = 0$ (the other parameters are gathered in Table 3).

where

$$A = a_{10}, \quad B = (a_{11} - a_{13}) \quad \text{and} \quad C = a_{12}.$$

The roots of Eq. (15) are

$$\lambda_1^* = \frac{-B - \sqrt{B^2 - 4AC\left(1 - \mathcal{R}_0^H\right)}}{2} \quad \text{and} \quad \lambda_2^* = \frac{-B + \sqrt{B^2 - 4AC\left(1 - \mathcal{R}_0^H\right)}}{2}. \tag{16}$$

The discriminant Δ of Eq. (15) can be written as a function of $\widetilde{\mathcal{R}_0^H}$, with $\widetilde{\mathcal{R}_0^H} = \mathcal{R}_0^H$, as

$$\Delta(\widetilde{\mathcal{R}_0^H}) = B^2 - 4AC\left(1 - \widetilde{\mathcal{R}_0^H}\right).$$

Note that

$$\frac{d\Delta(\widetilde{\mathcal{R}_0^H})}{d\widetilde{\mathcal{R}_0^H}} = 4AC$$

so that the function $\widetilde{\mathcal{R}_0^H} \mapsto \Delta(\widetilde{\mathcal{R}_0^H})$ is increasing on $(-\infty, +\infty)$.

Solving the algebraic equation in $\widetilde{\mathcal{R}_0^H}$, $\Delta(\widetilde{\mathcal{R}_0^H}) = 0$, we obtain the unique solution

$$\mathcal{R}_0^{H*} = \frac{4AC - B^2}{4AC} = 1 - \frac{B^2}{4AC} < 1. \tag{17}$$

Given the fact that $\Delta(\widetilde{\mathcal{R}_0^H})$ is increasing, one has

$0 = \Delta(\mathcal{R}_0^{H*}) < \Delta(\widetilde{\mathcal{R}_0^H})$ for any $\widetilde{\mathcal{R}_0^H} \in (\mathcal{R}_0^{H*}, 1)$.

- Assume in Eq. (17) that $\frac{B^2}{4AC} < 1$. Then $\mathcal{R}_0^{H*} > 0$. Thus, for $\widetilde{\mathcal{R}_0^H} \in (\mathcal{R}_0^{H*}, 1)$, the quadratic Eq. (15), where $\mathcal{R}_0^H$ is replaced by $\widetilde{\mathcal{R}_0^H}$ has two positive roots, given by (16) whenever $B < 0$, while there exists no positive solution for $B \geq 0$. The former case shows the possible existence of a backward bifurcation for Model (2).
- Assume in Eq. (17) that $\frac{B^2}{4AC} \geq 1$. Then $\mathcal{R}_0^{H*} < 0$ and Eq. (15) has two positive equilibria if $B < 0$ and $\widetilde{\mathcal{R}_0^H} \in (\mathcal{R}_0^{H*}, 1)$, while when $B \geq 0$ and $\widetilde{\mathcal{R}_0^H} < 1$ Eq. (17) has no positive equilibrium. The former case shows the possible existence of a full backward bifurcation for Model (2) [41].
- Assume $\mathcal{R}_0^H > 1$. Then Eq. (15) has one positive solution given by λ_2 in Eq. (16) irrespective of the sign of B. This shows that Model (2) may undergo a forward bifurcation.

To summarize, we have established the following result:

Theorem 4.1.

1. *Model (14) always admits a unique disease-free equilibrium*

$$E_0 = (S_{10}, S_{20}, 0, 0, 0).$$

2. *If $\mathcal{R}_0^H > 1$, Model (14) has a unique positive equilibrium E^*.*
3. *For $\mathcal{R}_0^H \in (\mathcal{R}_0^{H*}, 1)$, Model (2) possesses 2 endemic equilibria if and only if $B < 0$.*

Remark 4.2.

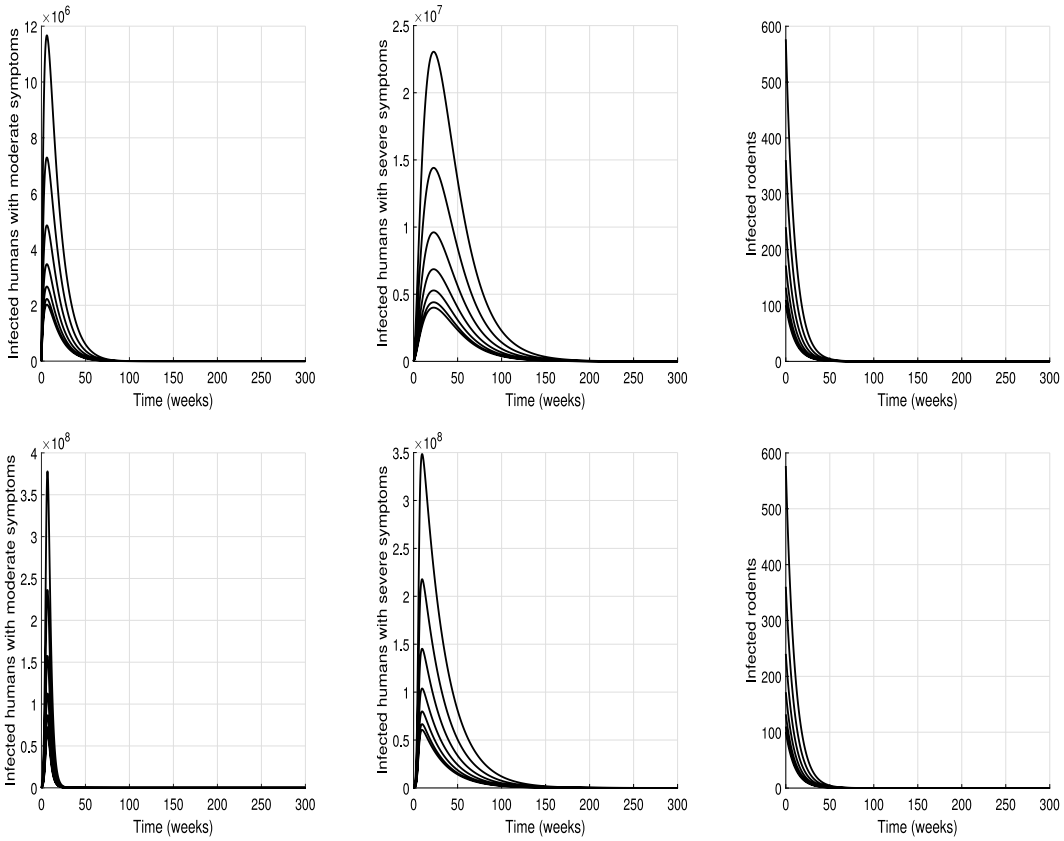

Fig. 6. GAS of the DFE for Model (2). Top three figures: case where $\mathcal{R}_0, \mathcal{R}_0^H, \mathcal{N} < 1$. Bottom three figures: case where $\mathcal{R}_0 < 1 < \mathcal{N}$ and $\mathcal{R}_0^H < 1$. The figures in the first row are plotted with $\beta_h = 0.088$ (the other parameters are as Table 3), which give $\mathcal{R}_0 = \mathcal{N} = 0.2261, \mathcal{R}_0^H = 3.1859 \times 10^{-4}$. Figures in the second row are plotted with the values in Table 3, which give $\mathcal{R}_0 = 0.226, \mathcal{R}_0^H = 0.00184$ and $\mathcal{N} = 8.3511$.

- It is evident that $\mathcal{R}_0^H$ represents the basic reproduction number for Model (14).
- The bifurcation diagram of Model (14) is shown in Fig. 3. This figure suggests that Model (14) can exhibit different bifurcation behaviors, including a forward bifurcation, a backward bifurcation, and a full backward bifurcation [41].
- In Theorem 4.1, item 1 and item 2 are straightforward. Item 3 involves the scenarios where a backward and a full backward bifurcation of the model exists. In the latter case, a LAS endemic equilibrium coexists with the disease-free equilibrium (DFE), which is also LAS. In this scenario, achieving global disease control is impossible. In the case of a backward bifurcation, one has to reduce and maintain $\mathcal{R}_0^H$ to be less than $\mathcal{R}_0^{H*}$ to achieve the global control of the disease.
- The parameter a_{13} can be expressed as an increasing function of a_3, such that $a_{13} = a_{13}(a_3)$ and $a_{13} = 0$ when the susceptibility parameter a_3 of PWH is zero. According to Eq. (9), quarantining PWH to reduce their infection risk eliminates the possibility of a backward bifurcation. Conversely, the likelihood of a backward bifurcation increases with higher susceptibility of PWH to infection. This underscores the importance of implementing S_2-control measures.

Theorem 4.3. *In the absence of the special group of PWH, the DFE of Model (2) is GAS when* $\mathcal{R}_0^H < 1$.

The proof of Theorem 4.3 is postponed to Appendix B.

For the general case, the global asymptotic stability of the DFE requires more conditions, as highlighted in the following result.

Theorem 4.4. *The DFE for Model (14) is globally asymptotically stable (GAS) provided that* $\mathcal{N}_0 < 1$.

The Proof of Theorem 4.4 can be done using the Lyapunov function L defined in Eq. (13) with $c_2 = 0$.

Regarding the stability of the unique endemic equilibrium for Model (14), one has the following result.

Theorem 4.5. *If* $\mathcal{R}_0^H > 1$ *but close to 1, the unique endemic equilibrium* E^* *of System (14) is locally asymptotically stable. Moreover, System (14) undergoes a trans-critical/forward bifurcation at* $\mathcal{R}_0^H = 1$.

Proof. Given the general complex form of System (14), it is appropriate to reduce it along the center manifold, parametrized by $(c(t), \phi)$, to a scalar differential equation of the form

$$\frac{dc}{dt} = \phi bc + ac^2$$

which determines the local dynamics of (14) in terms of the signs of the coefficients a and b that will be computed shortly (here $\phi := \mathcal{R}_0^H - 1$ is the bifurcation parameter).

We therefore use the center manifold theory as stated in Theorem C.1 to prove both statements.

Let us choose β_h as the bifurcation parameter and set β_h^* as the critical value of β_h. It is straightforward that $\mathcal{R}_0^H = 1$ if and only if

$$\beta^* = \frac{\phi_3\phi_4}{qc_1\phi_4 + \phi_3\nu_s c_3}.$$

To prove the local asymptotic stability of E^* and to be in the setting of [42], we consider the following notation.

$$x_1 = S_1, \quad x_2 = S_2, \quad x_3 = I_m, \quad x_4 = I_s, \quad x_5 = R.$$

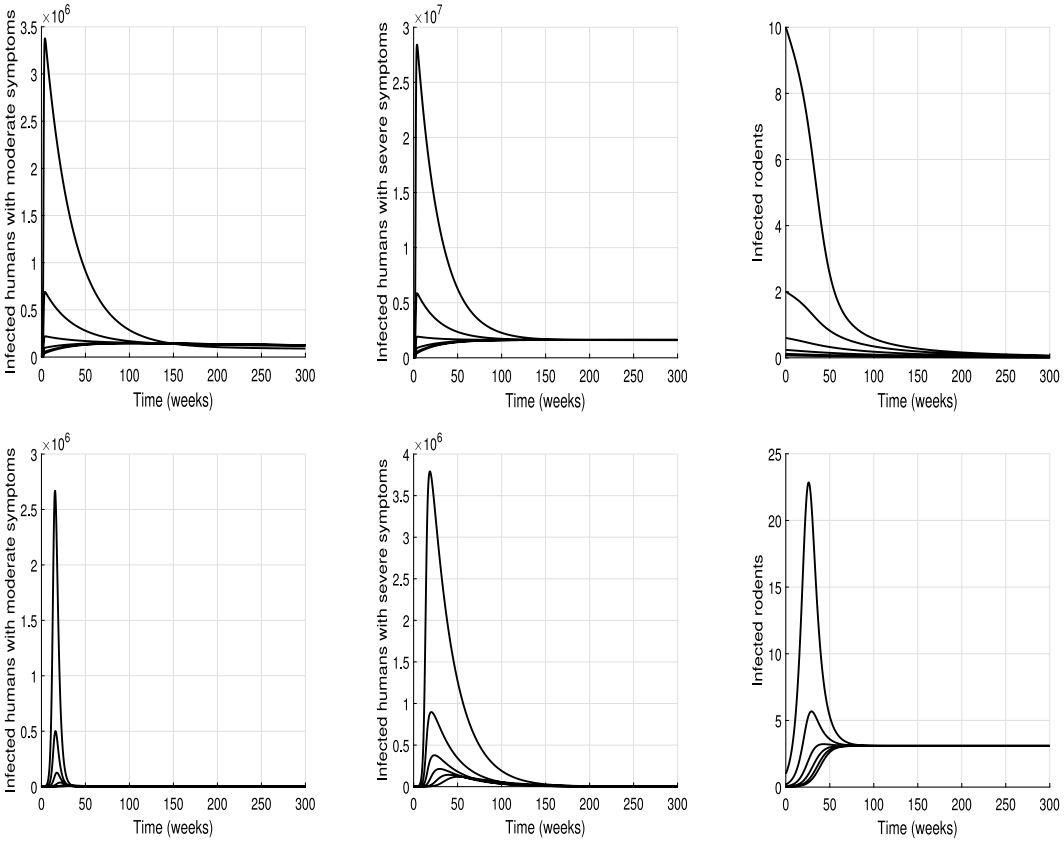

Fig. 7. Stability of the frontier equilibria for Model (2). The top three figures: the disease persists in the human population and disappears in the rodent population. Bottom three figures: the disease disappears in the human population, but persists in the rodent population. The figures in the first row are plotted with $\beta_r = 0.15, \beta = 4, \nu_s = 0.86, \gamma_m = 0.04, \sigma = 2.2, \delta = 0.0388$ leading to $\mathcal{R}_H = 1.9767 > 1$ and $\mathcal{R}_0^R = 0.9494 < 1$. The figures in the second row are plotted with $\beta_r = 0.3572, \omega = 0$ leading to $\mathcal{R}_0^R = 2.2608 > 1$ and $\mathcal{R}_0^H = 0.00184 < 1$ (the other parameters are as Table 3).

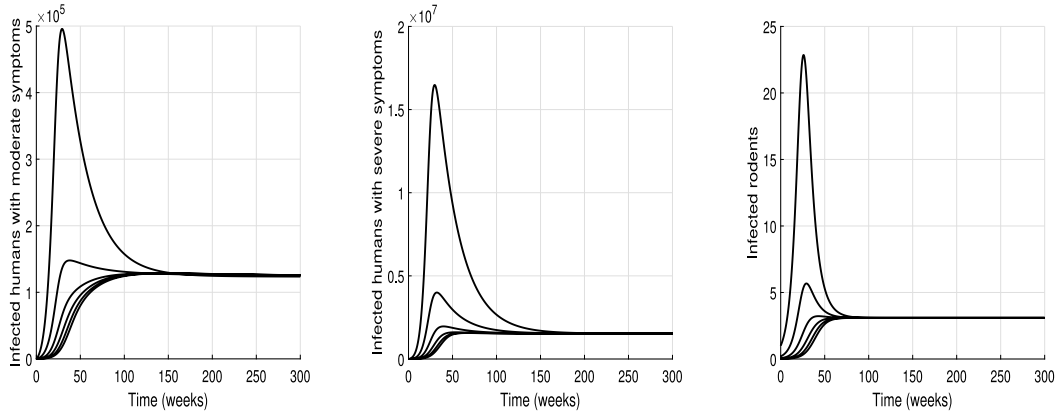

Fig. 8. Stability of the interior equilibrium. These figures are plotted when $\mathcal{R}_0^R > 1$. We used the parameters value $q = 0.13, \delta = 0.0388, \beta_r = 0.3572, p = 0.8, \gamma_m = 0.04656$ and $\gamma_s = 0.04466$ (the other parameters are as Table 3). With these parameters, one has $\mathcal{R}_0^R = 2.2608, \mathcal{R}_0^H = 0.0137$.

Then, System (14) takes the form

$$\frac{dx}{dt} = f(x),$$

where $f = (f_1, f_2, f_3, f_4, f_5)$ is defined as in the proof of Theorem 3.1.

The Jacobian matrix J of (14) at the DFE of Model (14) when $\beta = \beta^*$ is given by:

$$J = \begin{pmatrix} -\phi_1 & 0 & -\beta_h^* c_1 & -\beta_h^* \nu_s c_1 & 0 \\ \theta & -\phi_2 & -\beta_h^* a_3 c_2 & -\beta_h^* a_3 \nu_s c_2 & 0 \\ 0 & 0 & q\beta_h^* c_1 - \phi_3 & q\beta_h^* \nu_s c_1 & 0 \\ 0 & 0 & \beta_h^* c_3 & \beta_h^* \nu_s c_3 - \phi_4 & 0 \\ 0 & 0 & \gamma_m & \gamma_s & -\eta \end{pmatrix},$$

with

$$c_1 = \frac{S_{10}}{N_0},\ c_2 = \frac{S_{20}}{N_0} \text{ and } c_3 = \frac{(1-q)S_{10} + a_3 S_{20}}{N_0}.$$

To complete the proof, we need use the theorem stated in Theorem C.1:

- We claim that 0 is a simple eigenvalue of J and all the other eigenvalues of J have negative real parts.
  Obviously, $-\eta, -\phi_2, -\phi_1$ are eigenvalues of J. The remaining eigenvalues of J are those of the matrix.

$$\widehat{J} = \begin{pmatrix} q\beta_h^* c_1 - \phi_3 & q\beta_h^* \nu_s c_1 \\ \beta_h^* c_3 & \beta_h^* \nu_s c_3 - \phi_4 \end{pmatrix}.$$

The characteristic polynomial $P(X)$ of $\widehat{J}$ is given as

$$P(X) = X^2 - [q\beta_h^* c_1 - \phi_3 + \beta^* \nu_s c_3 - \phi_4]X + (q\beta_h^* c_1 - \phi_3)(\beta_h^* \nu_s c_3 - \phi_4) - \beta_h^{*2} c_3 q \nu_s c_1.$$

A simple computation shows that

$$(q\beta_h^* c_1 - \phi_3)(\beta_h^* \nu_s c_3 - \phi_4) - \beta_h^{*2} c_3 q \nu_s c_1 = 0.$$

Confirming that 0 is an eigenvalue of J. The last eigenvalue of J is given as

$$\lambda_0 = \beta_h^*(qc_1 + \nu_s c_3) - (\phi_3 + \phi_4) = \frac{-\phi_3^2 \nu_s c_3 - \phi_4^2 c_1 q}{qc_1\phi_4 + \phi_3 \nu_s c_3}.$$

Hence, the first claim is proved.

- The eigenvalues 0 has a right-eigenvector, $w = (w_1, w_2, w_3, w_4, w_5)^T$, and a left-eigenvector, $u = (u_1, u_2, u_3, u_4, u_5)^T$, given by:

$$\begin{cases} w_3 > 0;\ w_4 = \dfrac{\beta_h^* c_3 w_3}{\phi_4 - \beta_h^* \nu_s c_3} = \dfrac{\beta_h^* c_3 w_3 (qc_1\phi_4 + \phi_3 \nu_s c_3)}{qc_1\phi_4^2};\ w_5 = \dfrac{\gamma_m w_3 + \gamma_s w_4}{\eta} \\ w_1 = -\dfrac{\beta_h^* c_1 (w_3 + \nu_s w_4)}{\phi_1},\ w_2 = \dfrac{\theta w_1 - \beta_h^* a_3 c_2 (w_3 + \nu_s w_4)}{\phi_2}; \\ u_1 = u_2 = u_5 = 0;\ u_3 > 0;\ u_4 = \dfrac{q\beta_h^* \nu_s c_1 u_3}{\phi_4 - \beta_h^* \nu_s c_3} = \dfrac{q\beta_h^* \nu_s c_1 u_3 (qc_1\phi_4 + \phi_3 \nu_s c_3)}{qc_1\phi_4^2} \end{cases}$$

Thus,

$$u_i = 0,\ i = 1, 2, 5,\ u_3, u_4, w_3, w_4, w_5 > 0 \text{ and } w_1, w_2 < 0. \tag{18}$$

- The bifurcation coefficients as defined in Theorem C.1 given by

$$a = \sum_{k,i,j=1}^{8} u_k w_i w_j \frac{\partial^2 f_k}{\partial x_i \partial x_j}(0,0) \quad \text{and} \quad b = \sum_{k,i=1}^{5} u_k w_i \frac{\partial^2 f_k}{\partial x_i \partial \beta^*}(0,0).$$

Computing the involved partial derivatives, we have

$$\begin{aligned} a &= -2N_0^{-2}\beta_h^* q u_3 S_{10}[w_3 w_4(1 + \nu_s) + w_3^2 + \nu_s w_4^2] \\ &\quad - 2N_0^{-2}\beta_h^* u_4[((1-q)S_{10} + a_3 S_{20})(w_3 w_4(1 + \nu_s) + w_3^2 + \nu_s w_4^2)] \\ &< 0 \text{ by (18)} \end{aligned}$$

$$\begin{aligned} b &= u_3 S_{10} N_0^{-1} q(w_3 + \nu_s w_4) + u_4 S_{20} N_0^{-1}[((1-q) + a_3)(w_3 + \nu_s w_4)] \\ &> 0 \text{ by (18)}. \end{aligned}$$

Given the three bullets, the assumptions of Theorem C.1 are met to conclude that the unique endemic equilibrium E^* for Model (14) is LAS when $\mathcal{R}_0^H > 1$, but close to 1, and Model (14) undergoes a trans-critical bifurcation at $\mathcal{R}_0^H = 1$. □

5. Model calibration: Case of the USA

In this section, we calibrate Model (2) using the weekly cumulative Mpox cases in the USA from the beginning of the outbreak (10 May 2022) to 09 July 2024 (114 weeks) [43]. Given the population of HIV-infected individuals in the USA provided in [44], we set $S_2(0) = 1,200,000$. In 2022, the total population of the USA was estimated at $N_0 = 341,534,046$ [45]. On 10 May 2022, only one Mpox case was declared and was followed in the hospital. Thus, we set $S_1(0) = 341,534,046 - 1,200,000 - 1 = 340,334,045$. On the other hand, the population of rats in the USA in 2024 was estimated at 150,500,000 [46]. For simplicity, we take $S_r(0) = 150,000,000$. Due to the difficulty in estimating the number of infected rodents, we consider $I_r(0)$ as a parameter that will be obtained through the curve fitting. The initial conditions used for the calibration are gathered in Table 2.

Using the value of the mortality rate $\mu = 1/(76.4 \times 52)$ given in [13], we estimate the recruitment constant Λ as $\Lambda = N_h(0)\mu = (341,534,046)/(76.4 \times 52) = 85968.095$. Moreover, we assume that all PWH are under antiretroviral therapy. This, as in [22], allows us to estimate the death due to HIV, δ, and the death or Mpox recovered individuals, η, as $\delta = 0$ and $\eta = \mu$. According to [19], the Mpox death rate is 0.2 per year, thus τ can be estimated as $0.2/52 = 0.00385$. The rest of the parameters are obtained by calibration.

The calibration of the model, using the Nonlinear Least Squares fitting method, implemented by the "fminsearchbn" function in Matlab Software, is given in Fig. 4(a), and the estimated parameter values are provided in Table 3. Fig. 4(a) indicates that Model (2) excellently fits the Mpox outbreak in the USA. The parameters used give $\mathcal{R}_0^H = 0.0018$, and $\mathcal{R}_0^R = 0.226$. This highlights that Mpox will be overcome, at least locally, in rodent and human populations. The analysis reveals evidence of rodent-to-human Mpox transmission in the USA, consistent with the findings in [13].

The predicting curve plotted in Fig. 4(b) suggests that towards May 2027, Mpox will be overcome with 35,811 cases.

Because several Mpox cases will be registered in the meantime, it is necessary to implement control measures to reduce the incidence of the outbreak.

Table 2
Initial condition for the calibration.

$S_1(0)$	$S_2(0)$	$I_m(0)$	$I_s(0)$	$R(0)$	$S_r(0)$
340,334,045	1,200,000	0	1	0	150,000,000

Table 3
Parameters values and $I_r(0)$ obtained through calibration.

Parameters	Values	Units	Source
μ	$1/(76.4 \times 52)$	week^{-1}	[13]
Λ	85 968.095	hum.week^{-1}	Estimated
β_h	2.08856	week^{-1}	Fitted
β_r	0.03572	week^{-1}	Fitted
ω	0.3619	week^{-1}	Fitted
ν_s	0.0086	–	Fitted
p	0.166	–	Fitted
q	0.913	–	Fitted
θ	0.144	week^{-1}	Fitted
δ	0	week^{-1}	Estimated
σ	0.215	–	Fitted
η	$1/(76.4 \times 52)$	week^{-1}	Estimated
γ_m	0.4656	week^{-1}	Fitted
γ_s	0.0446	week^{-1}	Fitted
μ_r	0.158	week^{-1}	Fitted
Λ_r	0.8758	rod.week^{-1}	Fitted
τ	0.05598	week^{-1}	Estimated
$I_r(0)$	80 046	rodents	Fitted

6. Nonstandard finite difference (NSFD) scheme for model (2) and numerical simulations

6.1. NSFD scheme for model (2)

As highlighted in [47], the NSFD method was initiated more than three decades ago by Mickens. The authors of [47] go on to paraphrase Mickens [25] as follows: The NSFD method is becoming an established field whose concept of dynamic consistency and associated techniques is increasingly and quickly accepted for the construction of reliable numerical schemes for differential equations. More precisely, the advantage of the NSFD scheme is to preserve the stability of the equilibria, the boundedness, and the positivity of solutions.

Let

$$X^n = (S_1^n, S_2^n, I_m^n, I_s^n, R^n, S_r^n, I_r^n)^T,$$

denote an approximation of the solution

$$X(t_n) = (S_1(t_n), S_2(t_n), I_m(t_n), I_s(t_n), R(t_n), S_r(t_n), I_r(t_n))^T$$

at the discrete time $t = t_n = n\Delta t$, $n \in \mathbb{N}$, where $h = \Delta t > 0$ is the step size. We use the nontrivial denominator function φ of the discrete derivative

$$\varphi \equiv \varphi(h) = \frac{1 - e^{-kh}}{k} = h + \mathcal{O}(h^2), \text{ with } k \geq \mu + \delta + \eta, \tag{19}$$

where the parameter k captures the dynamics of the model. Our NSFD scheme reads as

$$\begin{cases} \frac{S_1^{n+1}-S_1^n}{\varphi} = p\Lambda - \lambda^n S_1^{n+1} - (\mu+\theta)S_1^{n+1}, \\ \frac{S_2^{n+1}-S_2^n}{\varphi} = (1-p)\Lambda + \theta S_1^{n+1} - \lambda^n a_3 S_2^{n+1} - (\mu+\delta)S_2^{n+1}, \\ \frac{I_m^{n+1}-I_m^n}{\varphi} = q\lambda^n S_1^{n+1} - (\mu+\gamma_m)I_m^{n+1}, \\ \frac{I_s^{n+1}-I_s^n}{\varphi} = (1-q)\lambda^n S_1^{n+1} + \lambda^n a_3 S_2^{n+1} - (\mu+\gamma_s+\tau)I_s^{n+1}, \\ \frac{R^{n+1}-R^n}{\varphi} = \gamma_m I_m^{n+1} + \gamma_s I_s^{n+1} - \eta R^{n+1}, \\ \frac{S_r^{n+1}-S_r^n}{\varphi} = \Lambda_r - \lambda_r^n S_r^{n+1} - \mu_r S_r^{n+1}, \\ \frac{I_r^{n+1}-I_r^n}{\varphi} = \lambda_r^n S_r^{n+1} - \mu_r I_r^{n+1}, \end{cases} \tag{20}$$

where

$$\lambda^n = \frac{\beta_h(I_m^n + \nu_s I_s^N)}{N_h^n} + \frac{\omega I_r^n}{N_r^n} \quad \text{and} \quad \lambda_r^n = \frac{\beta_r I_r^n}{N_r^n}. \tag{21}$$

Remark 6.1. Apart from the presence of a nontrivial denominator function φ (Mickens' Rule 2), the NSFD scheme (22) complies with Mickens' Rule 3 of discretizing the nonlinear terms in the right-hand side of Model (2) by nonlocal approximations [24,25], e.g.

$\lambda(t)S_1(t) \simeq \lambda^n S_1^{n+1}$ instead of $\lambda^n S_1^n$ or $\lambda^{n+1}S_1^{n+1}$.

To be more precise, (22) is a forward–backward Euler NSFD scheme whose implementation is done by the following Gauss–Seidel cycle, which results from further simplifications of (22).

$$\begin{cases} S_1^{n+1} = \frac{p\varphi\Lambda + S_1^n}{1+\varphi(\lambda^n+\phi_1)}, \\ S_2^{n+1} = \frac{(1-p)\varphi\Lambda + \varphi\theta S_1^{n+1} + S_2^n}{1+\varphi(\lambda^n a_3+\phi_2)}, \\ I_m^{n+1} = \frac{q\varphi\lambda^n S_1^{n+1} + I_m^n}{1+\varphi\phi_3}, \\ I_s^{n+1} = \frac{(1-q)\varphi\lambda^n S_1^{n+1} + \lambda^n a_3\varphi S_2^{n+1} + I_s^n}{1+\varphi\phi_4}, \\ R^{n+1} = \frac{\varphi(\gamma_m I_m^{n+1} + \gamma_s I_s^{n+1}) + R^n}{1+\varphi\eta}, \\ S_r^{n+1} = \frac{\varphi\Lambda_r + S_r^n}{1+\varphi(\lambda_r^n+\mu_r)}, \\ I_r^{n+1} = \frac{\varphi\lambda_r^n S_r^{n+1} + I_r^n}{1+\varphi\mu_r}. \end{cases} \tag{22}$$

Hence, though being implicit in form (20), Eq. (22) shows the explicit implementation coordinate-wise of the NSFD scheme (20).

The next three results show the power of the NSFD scheme (20). The first result is the discrete analog of Theorem 3.1. It reads as follows, the proof being a consequence of the representation (22) and the discrete Gronwall inequality applied to the discrete conservation

$$\begin{cases} \frac{N^{n+1}-N^n}{\varphi} = \Lambda - \mu N^{n+1} - \delta S_2^{n+1} - (\eta-\mu)R^{n+1} \le \Lambda - \mu N^{n+1}, \\ \frac{N_r^{n+1}-N_r^n}{\varphi} = \Lambda_r - \mu N_r^{n+1}. \end{cases} \tag{23}$$

Theorem 6.2. *The NSFD (20) or (22) is dynamically consistent with respect to the structural properties stated in Theorem 3.1. More precisely, this NSFD is a discrete dynamical system on the same region Ω irrespective of the size of Δt.*

We will see in the next subsection that Theorem 6.2, and thus Theorem 3.1 does not hold for classical numerical schemes.

The second result is about the qualitative feature of the discrete-free fixed point (DFF) of the iterative Eq. (22). It reads as follows and is proved by the discrete analog of the Hartman-Grobman Theorem or the Lyapunov indirect method [30].

Theorem 6.3. *For $\mathcal{R}_0 \neq 1$, the NSFD scheme is elementary stable in the sense of [48]: that is the fixed points of the scheme (22) are exactly the equilibrium points of Model (2); and their stability properties are the same as those of the continuous model. More precisely, the DFF is locally asymptotically stable whenever $\mathcal{R}_0 < 1$ and unstable for $\mathcal{R}_0 > 1$.*

Finally, the third result is about the global stability of the DFF. Its proof, based on the discrete analog of Castillo-Chavez et al. [42] Theorem provided in [47], is postponed to Appendix D. The result reads as follows:

Theorem 6.4. *In the absence of the rodent-to-human transmission and of the special group of PWH, the DFF of Model (20) or (22) is GAS whenever $\mathcal{R}_0^H < 1$ for any value of Δt.*

6.2. Numerical simulations

In this section, we perform some simulations for Model (2) using the parameters provided in Table 3.

In Fig. 5, we compare the NSFD scheme with ODE 45 and ODE 15s. The first row of three figures, plotted using ODE 45 and ODE 15s, produces the same graphs. They highlight that the solution of the model can be negative, a fact that is not realistic. On the contrary, irrespective of the value of the time size Δt, the NSFD scheme used in the bottom row of three graphs preserves the positivity of the solutions in accordance with Theorem 3.1 and Theorem 6.2. This shows the superiority of the NSFD scheme over Runge–Kutta of order 4.

In Fig. 6, we illustrate the global asymptotic stability of the DFE. In the top row, we consider the case where $\mathcal{R}_0 < \mathcal{N} < 1$ while in the bottom row, we consider the case where $\mathcal{R}_0 < 1 < \mathcal{N}$. This figure shows that all the trajectories converge to 0, meaning in both cases that the DFE is GAS. This suggests that the condition in Theorem 3.6 for the global asymptotic stability of the DFE can be relaxed as $\mathcal{R}_0 < 1$.

In Fig. 7, we illustrate the global asymptotic stability of the frontier equilibria for Model (2). In the top row, we consider the case where $\mathcal{R}_0^R < 1$ and $\mathcal{R}_0^H > 1$. These figures highlight that the disease is eliminated in the rodent population, while it persists in the human population in accordance with the principle of competitive exclusion. This suggests that reducing the spillover event from rodents to humans is not enough to overcome the disease; human-to-human transmission alone can sustain the Mpox in the human population.

In the case where the rodent-to-human transmission rate, $\omega = 0$, it can be easily seen that when $\mathcal{R}_0^R > 1$ and $\mathcal{R}_0^H < 1$, Model (2) can have a frontier equilibrium where the disease circulates in the rodent population only. The global asymptotic stability of this equilibrium is illustrated in the bottom row of Fig. 7. Fig. 7 shows that Model (2) obeys the competitive exclusion principle.

Under the spillover event from rodents to humans, Theorem 3.4 shows that when $\mathcal{R}_0^R > 1$, Model (2) has at least one positive equilibrium. Fig. 8 suggests that the endemic equilibrium is GAS whenever $\mathcal{R}_0^R > 1$, meaning that whenever the disease is endemic in the rodent population, it is endemic in the human population as well, regardless of the value of $\mathcal{R}_0^H$.

In what follows, we investigate the influence of some parameters on the dynamics of the infected humans. The top row of Fig. 9 focuses on the variation of the HIV infection rate, θ. We choose for θ the values. $\theta = 0.1, \theta = 0.4, \theta = 0.8$ (this set of values will be assumed for the other change of parameters unless otherwise specified). The results show that when θ increases, the number of severe cases increases as well, while the number of moderate cases decreases. Considering that only severe cases may die from the disease, the latter observation shows the need

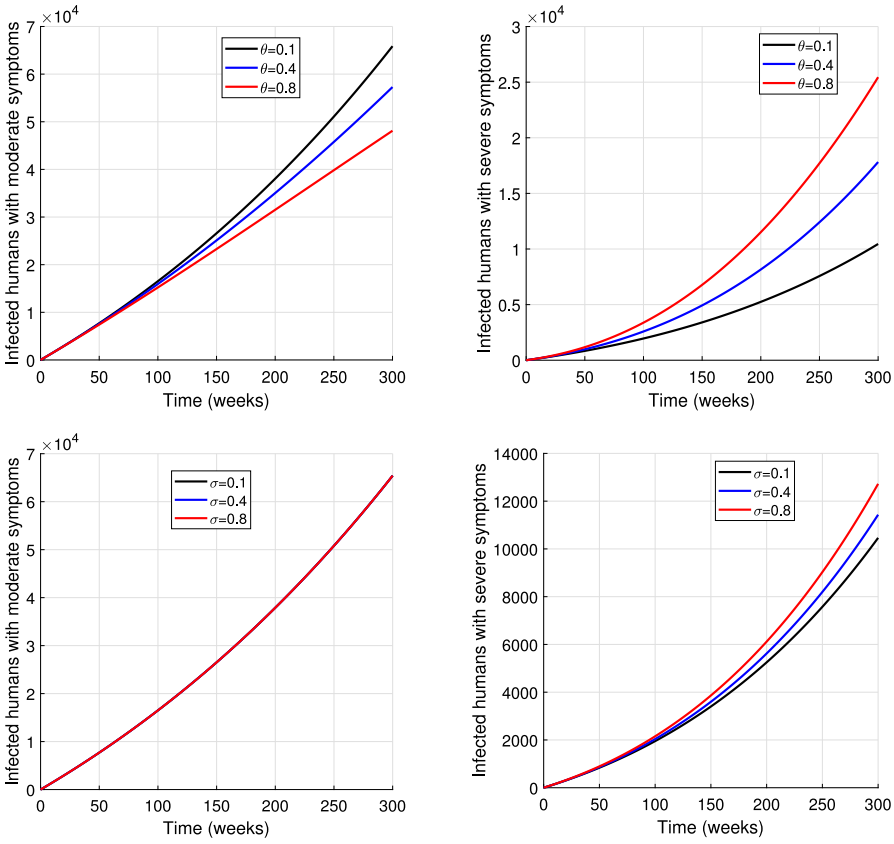

Fig. 9. Influence of the parameters σ and θ. The values of σ and θ are on the legend. The other parameters are as Table 3.

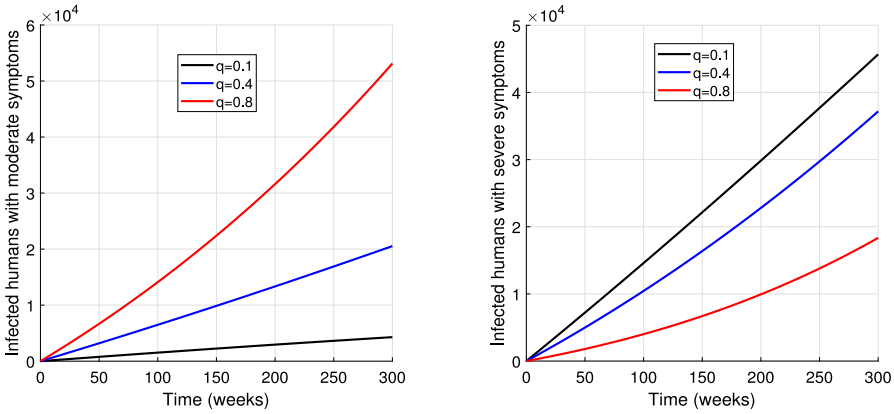

Fig. 10. Influence of the parameter q. The values of q are on the legend. The other parameters are as Table 3.

to reduce HIV transmission to mitigate the number of deaths due to Mpox. In the bottom row of Fig. 9, we investigate the influence of the modification parameter, σ, of the susceptibility of the individuals in S_2 as compared to those in S_1. This figure shows that increasing the value of σ does not influence the number of moderate cases (left plot) but increases the number of cases of severe Mpox (right plot). This underscores the need for intervention such as quarantine [38] or vaccination for HIV-susceptible individuals to prevent them from infection.

In Fig. 10, we vary the probability q for individuals in S_1 to develop a moderate form of the disease. As expected, when q increases, the number of infected with moderate symptoms increases, while those with severe symptoms decrease, showing that increasing the value of q will help decrease the number of deaths due to Mpox. To achieve this, one should strengthen the immune system of individuals in S_1 (by vaccination, for instance).

The low value of the modification of the contact rate ν between susceptible in S_1 and severe cases obtained through calibration suggests that most severe infected cases are isolated or self-isolated and so do not transmit much of the disease. In the top row of Fig. 11, we see that if Mpox severe infected cases mix in the population as the other individuals, the burden of the disease will increase in the I_s and I_m compartments.

In the bottom row of Fig. 11, we investigate the influence of the rodent-to-human transmission rate, ω, on the disease dynamic. We take $\omega = 0.001$, $\omega = 0.002$, and $\omega = 0.004$. This figure highlights that the number of infected individuals increases rapidly as ω increases, potentially leading to the disease becoming endemic. This explains the endemicity of Mpox in certain African countries, such as the DRC and

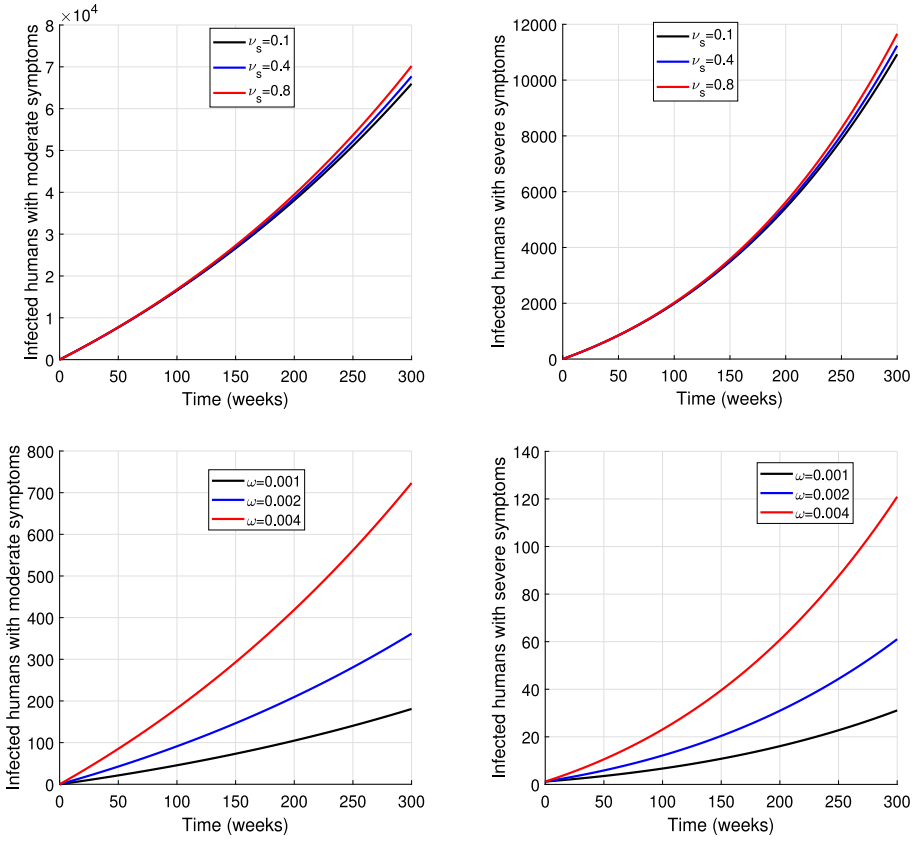

Fig. 11. Influence of the parameters ν and ω. This first row is plotted with $\tau = 0.1$ (the other parameters are as in Table 3).

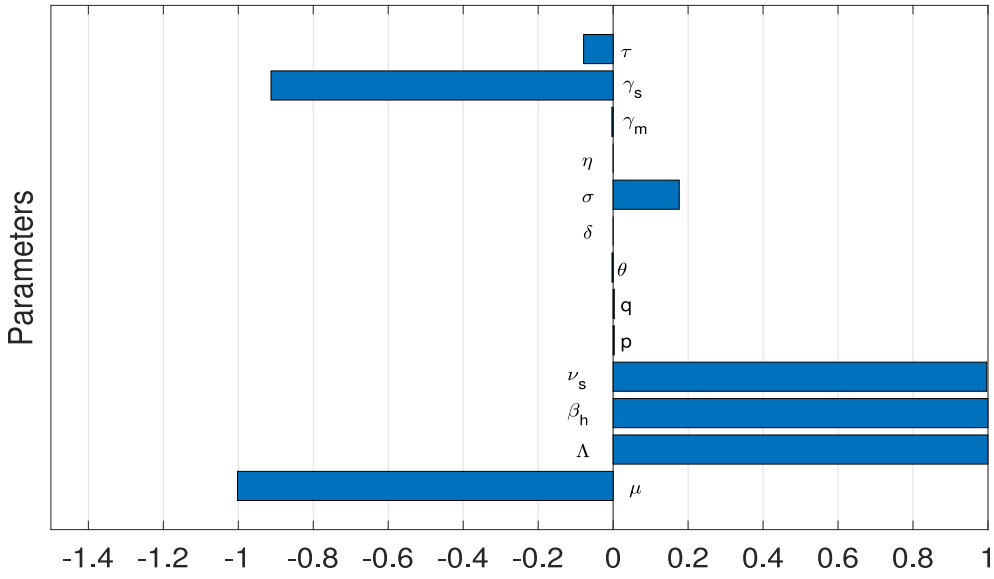

Fig. 12. Local sensitivity indices of $\mathcal{R}_0$.

Nigeria, and supports the findings in [49]. In these regions, controlling the disease in the rodent population and educating people about the dangers of handling and consuming rodents is an essential step towards combating the disease spread.

Furthermore, we address the local sensitivity analysis (LSA) of $\mathcal{R}_0^H$ to identify parameters that mostly drive the dynamics of Mpox within the human population. This analysis is important for designing control strategies against Mpox. The LSA of $\mathcal{R}_0^H$ can be measured using the forward normalized sensitivity index of $\mathcal{R}_0^H$ with respect to the model parameters. The LSA, $\varepsilon_a^{\mathcal{R}_0^H}$, of $\mathcal{R}_0^H$ at a parameter a is defined as [50,51]

$$\varepsilon_a^{\mathcal{R}_0^H} = \frac{\partial \mathcal{R}_0^H}{\partial a}\frac{a}{\mathcal{R}_0^H}.$$

A positive (negative) value of $\varepsilon_a^{\mathcal{R}_0^H}$ means that $\mathcal{R}_0^H$ is increasing (decreasing) with respect to a. The results of the LSA of $\mathcal{R}_0^H$ are represented

in Fig. 12. This figure highlights that β_h, ν_s, Λ and σ are the parameters that rapidly rise $\mathcal{R}_0^H$ whenever they increase. Thus the importance of reducing close contact with infected individuals, the migration rate, and strengthening the immune system of PWH (through vaccination, for instance). On the other hand, μ, γ_s, and τ are the most influential parameters that lead to a decreasing number of infected whenever they increase. This highlights the urgent need to develop a treatment against Mpox.

7. Conclusion

Mpox was declared a Public Health Emergency of International Concern (PHEIC) following the 2022 outbreak, which continues to progress. Several researchers report that the disease initially spread through contact with rodents, and subsequently through human-to-human transmission [3,4,13]. The latter transmission occurs during contact with skin lesions or other bodily fluids of infected individuals. Current reports on the ongoing outbreak show that the transmission and severity of Mpox are significantly influenced by whether the susceptible individuals are HIV-infected or not [6,12]. This has led us to focus on the spread of the disease with an emphasis on people living with HIV (PWH).

Hence, in this work, we proposed a model that allows individuals without HIV to develop either a severe or moderate form of Mpox, while individuals with HIV only exhibit the severe form of the disease when infected. From a mathematical perspective, we demonstrated the existence of at least one interior equilibrium when the disease is endemic in the rodent population. Additionally, we proved the existence of one or two positive frontier equilibria for the human-only sub-model when the basic reproduction number, $\mathcal{R}_0^H$, is less than one. This result indicates that even without considering rodent-to-human transmission, $\mathcal{R}_0^H < 1$ does not guarantee the elimination of the disease in humans, emphasizing the need for more extensive efforts in disease control.

In this context, we identified two threshold values $\mathcal{N}_0$ and $\mathcal{N}$, which, when kept below one, ensure the elimination of the disease in both the human-only and human-rodent populations. Given the high risk of Mpox for individuals with HIV, a targeted control strategy can focus on reducing transmission among this group. This strategy, termed S_2-control, can involve quarantining PWH or vaccinating them. We computed the threshold value that should be controlled to manage the disease by focusing on PWH specifically [36,37].

Furthermore, we calibrated our model using reported data from the USA [43]. This calibration indicated that our model closely aligns with the observed spread of the disease in the USA and suggested that human-to-human and rodent-to-human transmission of the disease are present in the population; however, the disease is not endemic. Projection estimates indicate that the disease is expected to be controlled by May 2027, with a projected total of 35,811 cases. This situation has prompted us to identify the factors that contribute to the burden of the disease within the human population. A local sensitivity analysis of the basic reproduction number $\mathcal{R}_0^H$ highlighted the critical need to reduce human-to-human transmission, develop effective treatment protocols, and strengthen the immune systems of people living with HIV (PWH).

The NSFD scheme we proposed supported the theory and revealed that rodent-to-human Mpox transmission is highly sensitive to the number of Mpox cases.

It is important to note that the model presented in this study did not account for the possibility of Mpox-infected individuals contracting HIV, nor did it explore the likelihood of co-infection by both diseases simultaneously. The latter aspect, which we are currently investigating, may be significant since both diseases share similar sexual transmission pathways. This would prevent the linear progression from the HIV-uninfected susceptible compartment to the HIV-susceptible one assumed in our model. Furthermore, Mpox has been reported in the USA following interactions with imported pet animals from Africa [13]. Therefore, it is also essential to examine the impact of human migrations and animal importation on Mpox transmission dynamics. More precisely, our future work on this topic includes the following.

1. The development of an HIV-Mpox co-infection model to investigate how the dynamics of one disease influence the dynamics of the other.
2. Investigating how human migration and animal importation drive Mpox spread.
3. Analysis of spatial and climate influences on disease transmission.
4. Identification of cost-effective control interventions to contain the disease transmission in both human and rodent populations.

CRediT authorship contribution statement

Arsène Jaurès Ouemba Tassé: Writing – review & editing, Writing – original draft, Visualization, Validation, Supervision, Software, Resources, Project administration, Methodology, Investigation, Formal analysis, Data curation, Conceptualization. **Yibetal Terefe:** Writing – review & editing, Writing – original draft, Supervision, Resources, Methodology, Investigation, Formal analysis, Conceptualization. **Jean Lubuma:** Writing – review & editing, Writing – original draft, Supervision, Resources, Methodology, Funding acquisition, Formal analysis, Conceptualization.

Declaration of competing interest

The authors declare that they have no conflict of interest.

Acknowledgments

The authors thank anonymous reviewers and the Handling Editor for their valuable suggestions that have helped improve the article. A.J. Ouemba Tassé and J.M.-S. Lubuma acknowledges the support of the National Research Foundation (NRF) under the Competitive Program for Rated Researchers (CPRR: Grant no. 138013). They also acknowledge the support of the University of the Witwatersrand under the Science Faculty Start-up Funds for Research and the Postdoctoral Program.

Appendix A. Notational parameters

$$\phi_1 = \mu + \theta,\ \phi_2 = \mu + \delta,\ \phi_3 = \mu + \gamma_m,\ \phi_4 = \mu + \gamma_s + \tau,\ a_1 = p\Lambda,$$
$$a_2 = (1-p)\Lambda,\ a_3 = 1 + \sigma,\ a_4 = 1 - q;\ a_5 = a_2\phi_1 + \theta a_1,\ a_6 = a_1a_4a_3 + a_2a_3,$$
$$a_7 = a_1a_4\phi_2 + a_3a_5,\ a_8 = \gamma_m q a_1 a_3\phi_4 + \phi_3\gamma_s a_6,\ a_9 = \gamma_m q a_1\phi_2\phi_4 + \phi_3\gamma_s a_7,$$
$$a_{10} = a_8 + a_6\eta\phi_3 + qa_1\eta\phi_4a_3,\ a_{11} = a_7\eta\phi_3 + a_9 + qa_1\eta\phi_2\phi_4 + a_2\eta\phi_3\phi_4 + a_1\eta a_3\phi_3\phi_4,$$
$$a_{12} = a_1\eta\phi_2\phi_3\phi_4 + a_5\eta\phi_3\phi_4,\ a_{13} = \beta_h q a_1\eta\phi_4a_3 + a_6\eta\phi_3\beta_h\nu_s,$$
$$a_{14} = \beta_h qa_1\eta\phi_4\phi_2 + a_7\eta\phi_3\beta_h\nu_s,$$
$$b_1 = \frac{((1-q)S_{10} + a_3S_{20})}{\phi_3},\ b_2 = \frac{((1-q)S_{10} + a_3S_{20})}{\phi_4},$$
$$b_3 = \frac{((1-q)S_{10} + a_3S_{20})}{\mu_r},$$
$$b_4 = ((1-q)S_{10} + a_3S_{20}),\ \phi_5 = \phi_4\gamma_m q + \phi_3\gamma_s(1-q),$$
$$\phi_6 = q\phi_4\mu + (1-q)\phi_3\mu + \phi_5,$$
$$N_0 = S_{10} + S_{20};\ c_1 = \frac{S_{10}}{N_0},\ c_2 = \frac{S_{20}}{N_0};\ c_3 = \frac{(1-q)S_{10} + a_3S_{20}}{N_0}.$$

Appendix B. Proof of global asymptotic stability of the DFE for model (14) in the absence of special group of PWH (Theorem 4.3)

Without the account of PWH, Model (14) becomes

$$\begin{cases} \dot{S}_1 = \Lambda - \lambda S_1 - \mu S_1, \\ \dot{I}_m = q\lambda S_1 - (\mu + \gamma_m) I_m, \\ \dot{I}_s = (1-q)\lambda S_1 - (\mu + \gamma_s + \tau) I_s, \\ \dot{R} = \gamma_m I_m + \gamma_s I_s - \mu R, \end{cases} \tag{B.1}$$

where

$$\lambda = \frac{\beta_h (I_m + \nu_s I_s)}{N_h},$$

and under this assumption,

$$\mathcal{R}_0 = \frac{q\beta_h}{\phi_3} + \frac{\beta_h \nu_s (1-q)}{\phi_4}, S_{10} = \frac{\Lambda}{\mu}.$$

We rewrite the model (B.1) as

$$\begin{cases} \dfrac{dX}{dt} = F(X,Y) \\ \dfrac{dY}{dt} = G(X,Y),\ G(X,0) = 0 \end{cases} \tag{B.2}$$

where $X = (S_1, R) \in \mathbb{R}^2$ and $Y = (I_m, I_s) \in \mathbb{R}^2$, with the components of $X \in \mathbb{R}^2$ denoting the non-infected population, and the components $Y \in \mathbb{R}^2$ denoting the infected population.

The DFE Q_0 of Model (B.1) can be denoted as $E_0 = (X^*, 0)$, $X^* = \left(\frac{\Lambda}{\mu}, 0\right)$.

The DFE is globally asymptotically stable if the following two conditions are satisfied [52]:

1. For the system $\dfrac{dX}{dt} = F(X,0)$, X^* is GAS.
2. $G(X,Y) = BY - \hat{G}(X,Y)$, $\hat{G}(X,Y) \geq 0$ for $(X,Y) \in \Omega$, where $B = D_Y G(X^*, 0)$ is a Metzler matrix and Ω is defined in Theorem 3.1.

From the System (B.1), one can easily see that,

$$B = \begin{pmatrix} q\beta_h - \phi_3 & q\nu_s\beta_h \\ (1-q)\beta_h & (1-q)\nu_s\beta_h - \phi_4 \end{pmatrix},$$

$$\hat{G}(X,Y) = \begin{pmatrix} q\beta_h(I_m + \nu_s I_s)\left(1 - \dfrac{S_1}{N_h}\right) \\ (1-q)\beta_h(I_m + \nu_s I_s)\left(1 - \dfrac{S_1}{N_h}\right) \end{pmatrix}.$$

Clearly, $\hat{G}(X,Y) \geq 0$ for $(X,Y) \in \Omega$. Moreover, it is evident that X^* is GAS for the system $\dfrac{dX}{dt} = F(X,0)$. Therefore, following the Theorem of Castillo-Chavez et al. presented in [52], the DFE of model (B.1) is GAS when $\mathcal{R}_0^H < 1$.

Appendix C. Theorem of Castillo-Chavez and Song [42] (theorem 4.1)

Theorem C.1. *Consider the following general system of ordinary differential equations with a parameter ϕ*

$$\frac{dx}{dt} = f(x,\phi), f : \mathbb{R}^n \times \mathbb{R} \mapsto \mathbb{R}^n \text{ and } f \in \mathbb{C}^2(\mathbb{R}^n \times \mathbb{R}) \tag{C.1}$$

Without loss of generality, it is assumed that 0 is an equilibrium for system (C.1) for all values of the parameter ϕ that is $f(0,\phi) = 0\ \forall\ \phi$. Moreover, let us assume

A1: $A = D_x f(0,0) = \left(\dfrac{\partial f_i}{\partial x_j}(0,0)\right)$ *is the linearization of system (C.1) around the equilibrium 0 with ϕ evaluated at 0. Zero is a simple eigenvalue of A and all other eigenvalues of A have negative real parts;*

A2: *Matrix A has a right eigenvector w and a left eigenvector v corresponding to the zero eigenvalue.*

Let f_k be the kth component of f and set

$$a = \sum_{k,i,j=1}^{n} v_k w_i w_j \frac{\partial^2 f_k}{\partial x_i \partial x_j}(0,0),$$

$$b = \sum_{k,i=1}^{n} v_k w_i \frac{\partial^2 f_k}{\partial x_i \partial \phi}(0,0). \tag{C.2}$$

The local dynamics of System (C.1) around 0 are determined by a and b.

(i) *$a > 0, b > 0$, when $\phi < 0$ with $|\phi| \ll 1$, 0 is locally asymptotically stable, and there exists a positive unstable equilibrium; when $0 < \phi \ll 1$, 0 is unstable and there exists a negative and locally asymptotically stable equilibrium;*

(ii): *$a < 0, b < 0$, when $\phi < 0$ with $|\phi| \ll 1$, 0 is unstable and there exists a positive unstable equilibrium;*

(iii): *$a > 0, b < 0$. When $\phi < 0$ with $|\phi| \ll 1$, 0 is unstable, and there exists a locally asymptotically stable negative equilibrium; when $0 < \phi \ll 1$, 0 is stable, and a positive unstable equilibrium appears;*

(iv) *$a < 0, b > 0$. When ϕ changes from negative to positive, 0 changes its stability from stable to unstable. Correspondingly a negative unstable equilibrium becomes positive and locally asymptotically stable.*

Appendix D. Proof of Theorem 6.4

Without the account of PWH, the human-to-human discrete Model (22) is equivalent to

$$\begin{cases} S_1^{n+1} = \dfrac{\varphi\Lambda + S_1^n}{1 + \varphi(\lambda^n + \mu)}, \\ I_m^{n+1} = \dfrac{q\varphi\lambda^n S_1^{n+1} + I_m^n}{1 + \varphi\phi_3}, \\ I_s^{n+1} = \dfrac{(1-q)\varphi\lambda^n S_1^{n+1} + I_s^n}{1 + \varphi\phi_4}, \\ R^{n+1} = \dfrac{\varphi(\gamma_m I_m^{n+1} + \gamma_s I_s^{n+1}) + R^n}{1 + \varphi\mu}. \end{cases} \tag{D.1}$$

The discrete dynamical system (D.1) on $\Omega \subset \mathbb{R}_+^2 \times \mathbb{R}_+^2$ of the form

$$X^{n+1} = F_h(X^n, Y^n), \tag{D.2}$$

$$Y^{n+1} = G_h(X^n, Y^n), \quad G_h(X^*, 0) = 0 \tag{D.3}$$

for $X^n = (S_1^n, R^n)$, $Y^n = (I_m^n, I_s^n)$ and $X^* = (\frac{\Lambda}{\mu}, 0)$.

Further computation of (D.2)–(D.3) can lead us to

1. For the subsystem (D.2), $X^{n+1} = F_h(X^n, 0) = \begin{bmatrix} \frac{\varphi\Lambda + S_1^n}{1+\mu\varphi} \\ 0 \end{bmatrix} = \begin{bmatrix} \frac{\Lambda}{\mu} + (S_1^0 - \frac{\Lambda}{\mu})\left(\frac{1}{1+\mu\varphi}\right)^n \\ 0 \end{bmatrix}$, the fixed equilibrium point X^* is globally asymptotically stable.
2. The second sub-system, (D.3), can be decomposed into

$$Y^{n+1} = G_h(X^n, Y^n) = A_h Y^n - \tilde{G}_h(X^n, Y^n),$$

where

$$A_h = \begin{bmatrix} \frac{1}{1+\varphi\phi_3} & 0 \\ 0 & \frac{1}{1+\varphi\phi_4} \end{bmatrix}$$

and

$$\tilde{G}_h(X^n, Y^n) = \beta_h(I_m^n + \nu_s I_s^n)\left(\frac{\varphi\Lambda + S_1^n}{N_h^n + \varphi(\beta_h(I_m^n + \nu_s I_s^n) + \mu N_h^n)}\right) B \geq 0,$$

with $B = \begin{bmatrix} \frac{q\varphi}{1+\mu\phi_3} \\ \frac{(1-q)\varphi}{1+\varphi\phi_4} \end{bmatrix}$.

Here A_h is a Metzler matrix with spectral radius $\rho(A_h) < 1$.

Using Theorem 5.3 in [47], we obtain $Y^n \leq (A_h)^n Y^0$ and infer that the fixed point $(X^*, 0)$ is globally asymptotically stable in Ω.

Data availability

Data will be made available on request.

References

[1] WHO, Mpox (monkeypox), 2023, (Mpox key facts). (Last access 20 August 2024).
[2] Institut Pasteur, Mpox (Variole de Singe), Mpox Zoonose, 2024, (Accessed on 20 August 2024).
[3] CDC, Mpox in animals and pets, 2024.
[4] Z.-K. Wei, Y.-C. Zhao, Z.-D. Wang, L.-Y. Sui, Y.-H. Zhao, Q. Liu, Animal models of mpox virus infection and disease, Infect. Med. 2 (2023) 153–166.
[5] Institut Pasteur, Monkeypox, 2024, (Accessed on 20 August 2024).
[6] C.S. Saldana, C.F. Kelley, B.M. Aldred, V.D. Cantos, Mpox and HIV: a narrative review, current HIV/AIDS reports, 2023, (Review on Mpox and HIV).
[7] WHO, Vaccines and immunization for Monkeypox: Interim guidance, 2022, (Vaccines and Immunization for Monkeypox).
[8] C. Wenham, M. Eccleston-Turner, Monkeypox as a PHEIC: Implications for global health governance, Lancet 400 (2022) 2169–2171.
[9] National Institute for Communicable Diseases (NICD), Mpox alert, 2024, (Accessed on 13 March 2025).
[10] B. Ortiz-Saavedra, E.S. Montes-Madariaga, C. Cabanillas-Ramirez, N. Alva, Epidemiologic situation of HIV and monkeypox coinfection: A systematic review, Coinfection: A Syst. Rev. Vaccines 11 (246) (2023) (HIV and Monkeypox Coinfection).
[11] VaccinesWork, Mpox is no longer officially a public health emergency; here's why we shouldn't let down our guard, 2023, (Mpox was not a PHEIC).
[12] CDC, Mpox and HIV, 2024, (Last access 20 August 2024).
[13] F.M. Allehiany, M.H. DarAssi, I, Ahmad, M.A. Khan, E.M. Tag-Eldin, Mathematical modeling and backward bifurcation in monkeypox disease under real observed data, Results Phys. 50 (2023) (Backward Bifurcation in an Mpox Model).
[14] T.D. Awoke, S.M. Kassa, Y.A. Terefe. M. D. Asfaw, Modeling on cost-effectiveness of monkeypox disease control strategies with consideration of environmental transmission effects in the presence of vaccination, Model. Earth Syst. Env. (2024) (Modeling Mpox with Environmental Transmission).
[15] A. Elsonbaty, W. Adel, A. Aldurayhim, A. El-Mesady, Mathematical modeling and analysis of a novel monkeypox virus spread integrating imperfect vaccination and nonlinear incidence rates, Ain Shams Eng. J. 15 (2024).
[16] M. Ngungu, E. Addai, A. Adeniji, U.M. Adam, K. Oshinubi, Mathematical epidemiological modeling and analysis of monkeypox dynamism with non-pharmaceutical intervention using real data from United Kingdom, Front. Public Heal. 11 (2023) (Mpox Dynamic with Non-Pharmaceutical Intervention).
[17] W. Okongo, J.O. Abonyo, D. Kioi, S.E. Moore, S.N. Aguegboh, Mathematical modeling and optimal control analysis of monkeypox virus in contaminated environment, Model. Earth Syst. Env. 10 (2024) 3969–3994.
[18] A. Omame, Q. Han, S.A. Iyaniwura, A. Ebenezer, N.L. Bragazzi, X. Wang, et al., Understanding the impact of HIV on Mpox transmission in the MSM population: A mathematical modeling study, Infect. Dis. Model. 9 (2024) 1117–1137.
[19] O.J. Peter, S. Kumar, N. Kumari, F.A. Oguntolu, K. Oshinubi, R. Musa, Transmission dynamics of monkeypox virus: a mathematical modelling approach, Model. Earth Syst. Env. (2021) (Transmission dynamics of Monkeypox virus).
[20] S.M. Garba, C.K. Mumba, Mathematical analysis of a model for the transmission dynamics of trichomonas vaginalis (TV) and HIV coinfection, Math. Methods Appl. Sci. 41 (2018) 8741–8764.
[21] Z. Mukandavire, A.B. Gumel, W. Garira, J.M. Tchuenche, Mathematical analysis of a model for HIV-Malaria co-infection, Math. Biosci. Eng. 6 (2009) 333–362.
[22] A. Omame, S.A. Iyaniwura, Q. Han, A. Ebenezer, N.L. Bragazzi, X. Wang, W.A. Woldegerima, J.D. Kong, Dynamics of mpox in an hiv endemic community: A mathematical modelling approach, Math. Biosci. Eng. 22 (2) (2025) 225–259.
[23] D. Xiao, W.H. Bossert, An intra-host mathematical model on interaction between HIV and malaria, Bull. Math. Biol. 72 (2010) 1892–1911.
[24] R.E. Mickens, Nonstandard Finite Difference Models of Differential Equation, World Scientific, Singapore, 1994.
[25] R.E. Mickens, Nonstandard Finite Difference Schemes: Methodology and Applications, World Scientific, Singapore, 2021.
[26] B. Ortiz-Saavedra, E.S. Montes-Madariaga, C. Cabanillas-Ramirez, N. Alva, A. Ricardo-Martinez, D.A. León-Figueroa, et al., Epidemiologic situation of HIV and monkeypox coinfection: A systematic review, Vaccines 11 (2023) 1–23.
[27] Epicentre Health Research, Everything you wanted to know about mpox, 2022, (Mpox overview). (Accessed on 03 December 2022).
[28] WHO, Mpox, 2025, (Mpox Overview).
[29] X. Liao, L. Wang, P. Yu, Stability of Dynamical Systems, Monograph Series on Nonlinear Science and Complexity, Vol. 5, Elsevier, Amsterdam, 2007.
[30] A. Stuart, A.R. Humphries, Dynamical Systems and Numerical Analysis, Vol. 2, Cambridge University Press, United Kingdom, 1998.
[31] P. Van den Driessche, J. Watmough, Reproduction numbers and sub-threshold endemic equilibria for compartment models of disease transmission, Math. Biosci. 180 (2002) 29–48.
[32] T. Berge, J. Lubuma, A.J. Ouemba Tassé, H.M. Tenkam, Dynamics of host-reservoir transmission of ebola with spillover potential to humans, Electron. J. Qual. Theory Differ. Equ. 14 (2018) 1–32.
[33] I. Lauko, G. Pinter, R.E. TeWinkel, Equilibrium analysis for an epidemic model with a reservoir for infection, Lett. Biomath. 5 (2018) 255–274.
[34] T. Malik, J. Reimer, A. Gumel, E. Elbasha, S. Mahmud, The impact of an imperfect vaccine and pap cytology screening on the transmission of human papillomavirus and occurrence of associated cervical dysplasia and cancer, Math. Biosci. Eng. 10 (2013) 1173–1205.
[35] L.P. LaSalle, The Stability of Dynamical Systems, Society for Industrial and Applied Mathematics, Philadelphia, 1976.
[36] Z. Shuai, J.A.P. Heesterbeek, P. van den Driessche, Erratum to: Extending the type reproduction number to infectious disease control targeting contacts between types, J. Math. Biol. 71 (2015) 255–257.
[37] Z. Shuai, J.A.P. Heesterbeek, P. van den Driessche, Extending the type reproduction number to infectious disease control targeting contacts between types, J. Math. Biol. 67 (2013) 1067–1082.
[38] M. Lipsitch, T. Cohen, B. Cooper, J.M. Robins, S. Ma, L. James, et al., Transmission dynamics and control of severe acute respiratory syndrome, Science 30 (2003) 1966–1970.
[39] HIVgov, Mpox and People with HIV, 2024.
[40] J.A.P. Heesterbeek, M.G. Roberts, The type-reproduction number T in models for infectious disease control, Math. Biosci. 206 (2007) 3–10.
[41] R. Ouifki, J. Banasiak, Epidemiological models with quadratic equation for endemic equilibria, Math. Methods Appl. Sci. (2020) 1–17, (Existence of Backward Bifurcation).
[42] C. Castillo-Chavez, B. Song, Dynamical models of tuberculosis and their applications, Math. Biosci. Eng. 1 (2) (2004) 361–404.
[43] CDC, (Mpox data for USA), 2023, (Accessed 03 October 2024).
[44] KFF, The HIV/AIDS epidemic in the United States: The basics, 2024, (HIV infected cases in USA).
[45] Worldometers, United States Population, 2025, (U.S. Population). (Accessed on 17 February 2025).
[46] World population review, 2025, (Population of Rodents in USA). (Accessed on 17 February 2025).
[47] M. Chapwanya, J. Lubuma, Y. Terefe, B. Tsanou, Analysis of war and conflict effect on the transmission dynamics of the tenth ebola outbreak in the democratic Republic of Congo, Bull. Math. Biol. 84 (2022) 136.
[48] R. Anguelov, T. Berge, M. Chapwanya, J.K. Djoko, P. Karma, J.M.-S. Lubuma, Y. Terefe, Nonstandard finite difference method revisited and application to the ebola virus disease transmission dynamics, Differ. Equ. Appl. 26 (6) (2020) 818–854.
[49] I. Adetifa, J.-J. Muyembe, D.G. Bausch, D.L. Heymann, Mpox neglect and the smallpox niche: a problem for Africa, a problem for the world, Lancet 401 (10390) (2023) 1822–1824.
[50] T. Berge, A.J. Ouemba Tassé, H.M. Tenkam, Mathematical modeling of contact tracing as a control strategy of Ebola Virus Disease, Int. J. Biomath. 11 (2018) 1850093–1–36.
[51] M. Martcheva, An Introduction to Mathematical Epidemiology, Springer, USA, 2015.
[52] C. Castillo-Chavez, Z. Feng, W. Huang, On the computation of R_0 and its role on global stability, in: C. Castillo-Chavez, S. Blower, P. Driessche, D. Kirschner, A.-A. Yakubu (Eds.), in: Mathematical Approaches for Emerging and Reemerging Infectious Diseases: An Introduction, vol. 125, Springer Science & Business Media, Berlin, 2002, pp. 229–250, (Role of R_0).